UNIVERSIDADE DE SÃO PAULO
INSTITUTO DE FÍSICA DE SÃO CARLOS

Lucas Prado Kamizaki

Studies of stochastic thermodynamics with optical tweezers

São Carlos

2022

Lucas Prado Kamizaki

Studies of stochastic thermodynamics with optical tweezers

Dissertation presented to the Graduate Program in Physics at the Instituto de Física de São Carlos, Universidade de São Paulo to obtain the degree of Master of Science.

Concentration area: Basic Physics

Advisor: Prof. Dr. Sérgio Ricardo Muniz

Corrected version
(Original version available on the Program Unit)

São Carlos
2022

Kamizaki, Lucas Prado
Studies of Stochastic Thermodynamics with Optical Tweezers / Lucas Prado Kamizaki; advisor Sérgio Ricardo Muniz - corrected version -- São Carlos 2022.
94 p.

Dissertation (Master's degree - Graduate Program in Theoretical and Experimental Physics) -- Instituto de Física de São Carlos, Universidade de São Paulo - Brasil , 2022.

1. Finite-time thermodynamics. 2. Optimal protocols. 3. Information-to-energy conversion. I. Muniz, Sérgio Ricardo, advisor. II. Title.

ACKNOWLEDGEMENTS

Parto do princípio de que não é necessário citar os nomes das pessoas que ajudaram, pois estas já sabem. Porém, seguindo a tradição, agradeço à minha família pelo suporte; ao meu orientador, professor Sérgio Muniz, pela oportunidade, liberdade, confiança e discussões; ao professor Marcus Bonança e ao Pierre Nazé pelas discussões e ensinamentos; à Thalyta e ao grupo do laboratório pelo suporte ao longo do processo; aos meus amigos Caio e Eduardo pelo companherismo; à Clara, não tenho palavras para expressar o quão grato sou a ela; e ao CNPq, Capes, e Fapesp pelo auxílio financeiro.

ABSTRACT

KAMIZAKI, L. P. **Studies of stochastic thermodynamics with optical tweezers**. 2022. 94p. Dissertation (Master in Science) - Instituto de Física de São Carlos, Universidade de São Paulo, São Carlos, 2022.

In the last thirty years, experimental and theoretical advancements allowed the investigation of the thermodynamics of small systems far from equilibrium. In 1998, Ken Sekimoto showed that work and heat can be associated with individual trajectories of a Brownian particle. In this context, work becomes a stochastic quantity with a probability distribution associated, respecting important relations as the Jarzynski equality. A paradigmatic study case in stochastic thermodynamics is the fluid-immersed particle trapped in a harmonic potential, a routinely achieved situation using optical tweezers. Using the light-matter interaction, optical tweezers can trap and control colloidal particles. Thus, optical tweezers are powerful and versatile tools when analyzing the thermodynamics of small systems. In this dissertation, we have simulated the dynamics of a colloidal particle trapped in an optical tweezer in different stochastic thermodynamic contexts. By simulating the experimental system, we can verify the feasibility and the adequate parameters to study stochastic thermodynamics in practice. The two main topics studied are optimization of protocols and information-to-energy conversion. Because the work probability density function depends on the protocol, different protocols have different average work values. Among all protocols with a certain intensity and duration, the one that stands out is the optimal protocol, i.e., the process that has the minimum average work. Generally, it is hard to find the optimal protocol analytically, and often other methods are necessary. The first main result is the numerical determination of the performance of the protocols found by approximate methods (for slowly varying processes and weak processes) for different protocol times and intensities. In addition to controlling the system through the protocol, information about its state allows Maxwell's demon-like experiments. The second main result is that we propose a new feedback experiment, simplifying the ideas presented in previous works. By doing so, we were able to calculate the dependency of the information-to-energy conversion and the delay time analytically. The simplifications made allow the study of feedback experiments using our actual experimental capabilities.

Keywords: Finite-time thermodynamics. Optimal protocols. Information-to-energy conversion.

RESUMO

KAMIZAKI, L. P. **Estudos de termodinâmica estocástica com pinças ópticas**. 2022. 94p. Dissertação (Mestrado em Ciências) - Instituto de Física de São Carlos, Universidade de São Paulo, São Carlos, 2022.

Nos últimos trinta anos, avanços experimentais e teóricos permitiram a investigação da termodinâmica de sistemas pequenos fora do equilíbrio. Em 1998, Ken Sekimoto mostrou que trabalho e calor podem ser associados a trajetórias individuais de uma partícula Browniana, e essas grandezas se tornam quantidade estocásticas com uma distribuições de probabilidade associadas. Um estudo de caso paradigmático em termodinâmica estocática é o de uma partícula imersa em um fluido e presa em um potencial harmônico, uma situação rotineiramente atingida com pinças ópticas. Usando as interações da luz com a matéria, pinças ópticas podem aprisionar e controlar partículas coloidais. Portanto, pinças ópticas são ferramentas poderasas e versáteis na análise da termodinâmica de sistemas pequenos. Nesta dissertação, nós simulamos a dinâmica de uma partícula coloidal aprisionada em uma pinça óptica em diferentes contextos da termodinâmica estocástica. Desta forma, nós pudemos verificar a viabilidade e os parâmetros adequados para realizar os experimentos na prática. Os dois principais tópicos estudados são de otimização de protocolos e a conversão informação-energia. Uma vez que a distribuição de probabilidade do trabalho depende do protocolo, diferentes protocolos terão valores médios para o trabalho distintos. Entre todos os protocolos, o nosso interesse esta no protocolo ótimo, isto é, o protocolo que possui o valor mínimo do trabalho médio. Geralmente é díficil encontrar expressões analíticas para o protocolo ótimo e, frequentemente, outros métodos são necessários. O primeiro resultado principal é que nós determinamos numericamente a performance de outros métodos (para processos lentos e para processos fracos) para diferentes tempos de protocolo e intensidades. Além do controle do sistema através do protocolo, a informação sobre o estado permite experimentos do tipo Demômio de Maxwell. O segundo resultado principal é a proposta de um novo experimento de *feedback*, simplificando as ideias apresentadas em trabalhos anteriores. Desta forma, nós conseguimos calcular a dependência da conversão informação-energia com o tempo de atraso. As simplificações feitas permitem o estudo de experimento de *feedback* com nossa capacidade experimental atual.

Palavras-chave: Termodinâmica em tempo finito. Protocolos ótimos. Conversão informação-energia.

LIST OF FIGURES

CONTENTS

1 INTRODUCTION

It has been 199 years since the breakthrough work by Nicolas Carnot (1), and, among the numerous advancements made during this period, we highlight the development of stochastic thermodynamics, which allows the treatment of small systems out of equilibrium. Stochastic thermodynamics extends concepts of classical thermodynamics to small systems, such as colloidal particles, single molecules, and atoms, unraveling and clarifying the properties of these systems.

1.1 Brief history

Classical thermodynamics is a phenomenological framework that explains the thermal properties of macroscopic systems.(2) Statistical mechanics tries to retrieve the thermodynamic properties by considering that systems are formed by many degrees of freedom. (3) Although Classical thermodynamics and Statical mechanics have different approaches, both treat systems in equilibrium and under quasistatic changes between equilibrium states.

However, processes occur at a finite time and rates become of crucial importance in describing the system's evolution. At the phenomenological level, irreversible thermodynamics covers the change between equilibrium states in a finite time, by using the concept of forces and fluxes. (2) Because it deals with finite time processes, the system can be out of equilibrium. In addition, at a statistical level, linear response theory deduces nonequilibrium quantities of a system subjected to an external field using measurements of equilibrium correlation functions.(4) Nonetheless, irreversible thermodynamics and linear response theory are only valid for processes close to equilibrium. Therefore, for a long time, exact results existed only for processes close to equilibrium, with the absence of universal analytical results for processes arbitrarily far from equilibrium. This situation drastically changed in the 90s.

Surprisingly, in 1997, Jarzynski deduced a relation connecting an equilibrium quantity, the free energy difference between states, with a nonequilibrium quantity, the average work required to change states. (5) This relation, known as the Jarzynski equality, is an analytical result for processes that drive the system arbitrarily far from equilibrium. Short after, a refinement came with Crooks's relation. (6) These results are the first fluctuations theorems for the work and are considered milestones in the development of Stochastic thermodynamics. Nowadays, there are several fluctuations theorems, and they differ in their range of validity, assumptions, and interpretations. (5–9) Another remarkable theoretical advancement in the development of Stochastic thermodynamics was due to Sekimoto in 1998. (10) He showed that work and heat can be associated with

the stochastic trajectory of a colloidal particle. These theoretical results together with advancements in the experiments made it possible to study the thermodynamics of small systems out of equilibrium. An example that appears over and over again is the DNA pulling experiments with optical tweezers. (11)

Stochastic thermodynamics is an emergent and vast field with many possibilities for study. We could examine the properties of nonequilibrium steady states (7), consider Brownian thermal machines and their efficiency at maximum power (the Novikov-Cuzborn-Ahlborn limit) (12–14), or the thermodynamics of biopolymers (DNA/RNA). (11) Here, the chosen itinerary was to investigate optimal protocols and the information-to-energy conversion. Optimal protocols are the processes that generate the minimum average work (15), while the information-to-energy conversion is the realization of Maxwell's demon-like experiments. (16) In the next section, we describe the organization of chapters and give some details of our journey.

1.2 Chapter's overview

In this dissertation, we study stochastic thermodynamics using simulations of a colloidal particle trapped in an optical tweezer. The first leading result is finding the performance of optimal protocols from linear response theory and slowly varying processes for different intensities and switching times. The second main result is the proposal of a new feedback experiment to be realized in our laboratory.

We begin in chapter 2, presenting the experimental system available in our laboratory. Although this dissertation has a computational/theoretical approach, the physical parameters chosen were experimentally motivated, based on the routinely made experiments.

Then, in chapter 3 we lay the theoretical foundations of the physical description with the Langevin equation and the Fokker-Planck equation. The former equation describes the individual trajectories, while the latter represents the evolution of the probability density function of the particle.

These two equations, however, do not introduce the classical thermodynamics concepts as work, heat, and entropy. So, in chapter 4, we present the ideas of the influential article (10) by Sekimoto. He has shown that work and heat can be associated with individual trajectories. Work becomes a stochastic quantity with a probability density function associated. The work distribution will depend on how we change the work parameter (the variable that the experimentalist has control), also known as a protocol. Different protocols will lead to different average values.

The optimal protocol is the one that has the smaller average work. For the particular case of a colloidal particle in a harmonic potential in the overdamped regime, the optimal

protocol was already analytically found.(15) Nonetheless, generally, encountering the optimal protocol is not an easy task. Thus, in chapter 5, we employed two linear response theory methods, one for slowly varying processes (17) and one phenomenological, to encounter the optimized processes. (18) The first main result of this dissertation is that we numerically verified the performance of these two approximate methods for different switching times and protocol intensities.

In chapter 6, we discuss the ideas behind Maxwell's demon experiment. (19) By simulating a particle in a double-well potential, we have been able to verify Landauer's principle. (20) Also, we reproduce the results of ref. (21), where the authors experimentally verified the information-to-energy conversion. Finally, we present our second main result: an experiment proposal, suitable for our optical tweezers setup, to verify the information-to-energy conversion.

2 OPTICAL TWEEZERS

Developed during the 1970s and 1980s by Arthur Ashkin (22–24) optical tweezers are helpful in different areas, from biological systems (25) to stochastic thermodynamics (26), allowing trapping and measurements of forces and torques with great precision. In the most basic configuration it contains a laser source and an objective lens with a high numerical aperture.

In this chapter, we present the basic theory of particle trapping by optical tweezers and the main features of the experimental system. The goal is to show the essential parameters to simulate it.

2.1 Basic theory

The physical phenomenon responsible for the functioning of optical tweezers is the radiation force. Historically, there are three ways to describe particle trapping, depending on the dimensions of the trapped particle d and the laser wavelength λ_{laser}.

- $d \ll \lambda_{laser}$ (Dipole approximation). In this limit, the particle is treated as a dipole in an electromagnetic field.
- $d \gg \lambda_{laser}$ (Ray optics regime). Geometrical optics can be utilized to describe the physical process.
- $d \approx \lambda_{laser}$ (Mie scattering). The former regimes greatly simplify the mathematical description. But in the intermediate case, complete wave-optical modeling of the particle-radiation interaction is necessary.

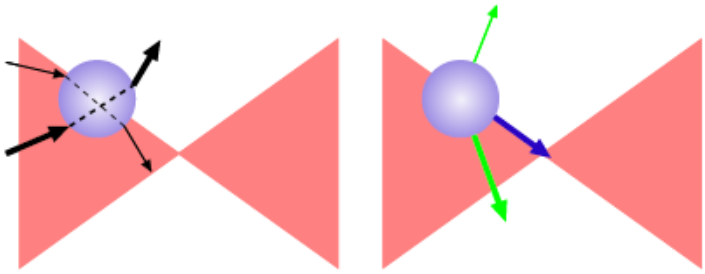

Figure 1 – The non-uniform intensity of the laser makes the momentum transfer by the outer ray smaller than that of the ray closer to the beam's center. The resultant effect, if $n_{particle} > n_{medium}$, is to trap the particle in the focal spot of the optical tweezers.

Source: Adapted from MARTINS (27)

The details of each description can be found in ref. (28) However, it is simpler to understand the phenomena through geometrical optics. Because light carries momentum and the particle's refractive index is different from the medium's refractive index, the ray suffers refraction and reflection when it impinges on the particle's surface, changing its direction. However, linear momentum needs to be conserved, so a change in the ray's direction means a transfer of momentum to the particle.

The intensity profile of the laser is spatially non-uniform, typically Gaussian, resulting in a non-even momentum transfer as shown in Figure 1. In other words, because the beam's intensity is greater at its center, more centralized rays will transfer more momentum than peripheric rays. As a consequence of Newton's third law, a net force in the direction of the trap's center if $n_{medium} < n_{particle}$ will arise.

2.1.1 Force exerted

Although the different descriptions of the colloidal particle trapping, the force exerted on the particle, in a first approximation, can be considered equal to $-\kappa(x - x_c)$, where κ is the trap's stiffness, and x_c is the trap's center position. Besides, a potential energy, $V(x)$, can be associated with this force, i.e.,

$$V(x) = \frac{\kappa}{2}(x - x_c)^2. \tag{2.1}$$

2.2 Experimental system

Here, we will briefly introduce the experimental system to support the parameters used in the simulations. For a complete discussion about the construction, calibration, and components, we refer to ref. (27) The essential idea is that we can control the power of the laser and its angular position through the acousto-optical modulator (AOM)(See Figure 2). Control of the laser's power allows changes of the trap stiffness, while the angular position determines the trap's center position, allowing the construction of different types of potentials (ex.: the double well). The physical observable is the position of the particle at time t, which is collected using the Quadrant Photodetector (QPD). The rate of position's acquisition reaches up to 150 kHz. Generally, the trapped particle is a silica sphere of 1 μm of radius, immersed in water at room temperature. The trap stiffness is of the order of some piconewtons per micrometer. In Table 1, the information about the physical constants that appears throughout this dissertation repeatedly is summarized.

2.2.1 Other potentials

In chapter 6, we will discuss the use of more complex potentials. Optical tweezers can accomplish such tasks by measuring the particle's position and changing the trap center very quickly. The harmonic potential is changed in a manner that, at each point

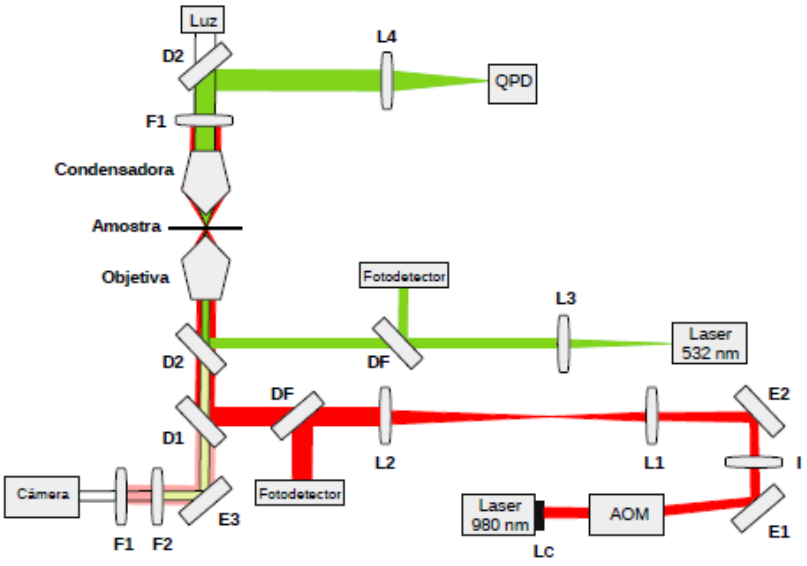

Figure 2 – Representation of the experimental system. The laser responsible for the trap has a wavelength 980 nm (in red), the acousto-optical modulator controls the position of the beam, and the QPD detects the particle's position. Generally, spherical silica particles with 1 μm of radius are trapped. The surrounding medium of the particle is water at room temperature.

Source: Adapted from MARTINS (27)

in space, it simulates the force of a more complex potential in the particle. Hence, this method creates a virtual potential that can be designed to achieve the experimentalist's goals. (29) The first experimental verification of Landauer's principle used this method. (30) If feedback control is not available, changing quickly the center's trap position can create certain potentials. (31)

Table 1 – Standard parameters. When the value of the physical parameter is not specified, it is assumed to have the value given in this table.

Physical quantity	Representation	Value	Observation
Particle's radius	r	1 μm	Spherical particle
Particle's density	ρ	2.65 g/cm^3	Silica
Particle's mass	m	11 pg	Calculated with $m = \frac{4}{3}\pi r^3 \rho$
Medium's viscosity	η	1.0 mPa · s	Water at 30 °C
Friction coefficient	γ	$1.885 \cdot 10^{-8}$ Ns/m	Calculated using Stokes' law $\gamma = 6\pi r\eta$
Medium's temperature	T	300 K	Room temperature
Initial trap stiffness	λ_i	1 pN/μm	Trap stiffness at the beginning of the protocol (See Chapter 4)
Final trap stiffness	λ_f	3 pN/μm	Trap stiffness at the end of the protocol
Acquisition's time	Δt	25 μs	Calculate as the inverse of the acquisition rate of the QPD

Source: By the author

3 BROWNIAN MOTION

3.1 Introduction

When observed through a microscope, our silica particle seems to move in a rapid random manner. This phenomenon is known as Brownian motion, and its explanation relies on the random forces that act due to the density fluctuations of the surrounding medium. The Brownian particle is a paradigmatic example in studying equilibrium and nonequilibrium processes. Mainly, there are two options to describe it: the Langevin equation and the Fokker-Planck equation. The first description is through Newton's second law with a stochastic term, and the second consists of a partial differential equation for the time evolution of the probability density.

In the previous chapter, we presented the experimental values of the physical constants adopted in our simulations. Here, we show the theoretical foundation of the physical description. The goals are to present the Langevin and Fokker-Planck equations and the article that is the basis for the simulations.

3.2 The Langevin Equation

If $x(t)$ is the position at time t of a small particle of mass m subjected to a potential $V(x)$ and immersed in a liquid with friction coefficient γ at temperature T, the equation of motion is given by

$$m\frac{d^2x(t)}{dt^2} = -\frac{d}{dx}V(x) - \gamma\frac{dx(t)}{dt} + \sqrt{2k_BT\gamma}\xi(t), \tag{3.1}$$

which is known as the Langevin equation. The last term on the right hand side, $\xi(t)$, is the stochastic term and represents the medium's density fluctuation. The stochastic force is a random gaussian white noise with zero mean. Mathematically, this can be put as

$$\overline{\xi(t)} = 0, \tag{3.2}$$

and

$$\overline{\xi(t)\xi(t')} = \delta(t - t'). \tag{3.3}$$

The over bars, $\overline{\cdot}$, represent averages under different realizations of the white noise.

3.2.1 Example 1: Free particle

For a free particle we have $V(x) = 0$, and the Langevin equation is written as

$$m\frac{d^2}{dt^2}x(t) = -\gamma\frac{d}{dt}x(t) + \sqrt{2k_BT\gamma}\xi(t). \tag{3.4}$$

It can be solved for $x(t)$ and $v(t)$ using the Laplace transform and the convolution integral. (32) Hence, the solutions are given by

$$x(t) = x_0 + \frac{m}{\gamma}(1 - e^{-\frac{\gamma t}{m}})v_0 + \sqrt{\frac{2k_BT}{\gamma}}\int_0^t \left[1 - e^{\frac{\gamma}{m}(t-s)}\xi(s)\right] ds, \tag{3.5}$$

and

$$v(t) = v_0 e^{-\frac{\gamma t}{m}} + \frac{\sqrt{2k_BT\gamma}}{m}\int_0^t e^{-\frac{\gamma}{m}(t-s)}\xi(s)ds, \tag{3.6}$$

where $x_0 = x(0)$ and $v_0 = v(0)$ are the initial position and velocity, respectively. It is noteworthy that we are using the Stratonovich integral throughout this dissertation.

An important approximation is found in the literature when the medium has high friction, or the particle's mass is low. This approximation is called the strong friction limit. It is interesting to calculate first the velocity autocorrelation function $\langle\overline{v(t)v(t')}\rangle_{eq}$, where the brackets, $\langle\ \cdot\ \rangle_{eq}$, represent the average over the thermal equilibrium distribution. This can be done using the expression above for the velocity, the properties of the stochastic term (eqs. (3.2) and (3.3)), and considering the equipartition theorem

$$\frac{m\langle v_0^2\rangle_{eq}}{2} = \frac{1}{2}k_BT. \tag{3.7}$$

Accordingly, the velocity autocorrelation function is equal to (3)

$$\langle\overline{v(t)v(t')}\rangle_{eq} = \frac{k_BT}{m}e^{-\frac{\gamma}{m}|t-t'|}. \tag{3.8}$$

It is noteworthy that the correlation function above decays exponentially as time increases, meaning that information about the initial velocity decays exponentially. The time scale in which the exponential decays is called the momentum relaxation time $\tau_M = m/\gamma$. If τ_M is small, the velocity of the Brownian particle relaxes to its equilibrium state very rapidly. As a consequence, the velocity of the particle reaches its stationary state quickly and $dv/dt \approx 0$. Thus, it is a good approximation to drop the inertial term in eq. (3.4), i.e.,

$$0 = -\gamma\frac{dx(t)}{dt} + \sqrt{2k_BT\gamma}\xi(t). \tag{3.9}$$

This in the Langevin equation in the strong friction limit and describes well our experimental setup. Because the acquisition time ($10 - 25$ μs) is much larger than the momentum relaxation time $\tau_M \approx 0.58$ μs, we do not measure the velocity of the particle relaxing to the equilibrium state. Therefore, justifying the use of the approximation.

3.2.2 Example 2: Harmonic potential

For a harmonic potential (eq. (2.1)) the procedure is the same of the previous example. However, in this case we will only calculate the position. The Langevin equation is written as

$$m\frac{d^2x(t)}{dt^2} = -\kappa x(t) - \gamma\frac{dx(t)}{dt} + \sqrt{2k_BT\gamma}\xi(t). \tag{3.10}$$

The solution can be found again using the Laplace transform. Hence, the solution for the overdamped regime ($\gamma^2 > 4m\kappa$) is given by

$$x(t) = \frac{1}{2\sqrt{\Delta}}(v_0 - s_2 x_0)e^{s_1 t} - \frac{1}{2\sqrt{\Delta}}(v_0 - s_1 x_0)e^{s_2 t} + \frac{\sqrt{k_B T\gamma}}{\sqrt{2\Delta}m}\int_0^t W(t')\mathcal{G}(t-t')dt' \quad (3.11)$$

with the following definitions

$$\Delta = \left(\frac{\gamma}{2m}\right)^2 - \frac{\kappa}{m}, \quad (3.12)$$

$$s_1 = -\frac{\gamma}{2m} + \sqrt{\Delta}, \quad (3.13)$$

$$s_2 = -\frac{\gamma}{2m} - \sqrt{\Delta}, \quad (3.14)$$

and

$$\mathcal{G}(t-t') = e^{s_1(t-t')} - e^{s_2(t-t')}. \quad (3.15)$$

Observe that the position of the particle decay exponentially in a time scale given by $1/s_1$ and $1/s_2$.

The solution (3.11) is essential to obtain the relaxation function of the problem that will allow us to find the optimal protocol in the linear response regime (see chapter 5.2.1).

3.2.3 A Finite Differential Algorithm for the Langevin equation

In undergraduate courses, it is common to learn how to simulate ordinary differential equations (ODEs). Nonetheless, stochastic differential equations have characteristics that demand more sophisticated simulation methods because of the discontinuities of the stochastic term and its infinite variation. (33) The simulations in this dissertation have as reference (34), which presents a way to simulate the Langevin dynamics using a finite differential algorithm.

This simulation of the dynamics can be done by approximating the solution $x(t)$ for a discrete-time sequence x_i which represents the solution at regular time steps $t_i = i\Delta t$. If the steps are small enough then it is a good approximation $x_i \approx x(t_i)$. In addition, the first and second time derivatives of the position are substitute by

$$\frac{dx(t)}{dt} \approx \frac{x_i - x_{i-1}}{\Delta t}, \quad (3.16)$$

and

$$\frac{d^2x(t)}{dt^2} \approx \frac{x_i - 2x_{i-1} + x_{i-2}}{\Delta t^2}, \quad (3.17)$$

respectively. Further, if there is a harmonic potential, the restoring force is substituted by,

$$\frac{dV(x)}{dx} = -\kappa x(t_i) \approx -\lambda x_i. \quad (3.18)$$

The idea is to build a recursion method, where given the position x_{i-2} and x_{i-1}, the value of x_i is determined. Given x_{i-1} and x_i, it is obtained x_{i+1} and so on. This first order integration represents a generalization of the Euler method to stochastic differential equations. Until now, nothing has changed compared to the treatment of ODEs. The fundamental idea to treat the stochastic term is to construct a discrete sequence of random numbers ξ_i that imitates the behavior of the stochastic term. Following the equations (3.2) and (3.3) this discrete sequence must satisfy

$$\overline{\xi_i} = 0 \tag{3.19}$$

and

$$\overline{\xi_i \xi_j} = \frac{\delta_{ij}}{\Delta t}. \tag{3.20}$$

Note that the variance of the distribution is $1/\Delta t$. It is useful to rescale ξ_i as

$$w_i = \xi_i \sqrt{\Delta t}. \tag{3.21}$$

The new sequence w_i has the same average, but its variance is equal to the unity. In our simulations, we utilized the Box-Muller algorithm to generate random numbers with a Gaussian distribution (with variance equal to 1) from a random number generator with outputs from 0 to 1. Here, we replace eqs. (3.16), (3.17), (3.18), and (3.21) , into (3.10), and obtain

$$x_i = \frac{(2m + \gamma \Delta t) x_{i-1} - m x_{i-2} + \sqrt{2 k_B T \gamma \Delta t^3} w_i}{m + \gamma \Delta t + \kappa \Delta t^2} \tag{3.22}$$

To correctly reproduce the dynamics of the colloidal particle, the time step must be much smaller than the relaxation time ($\tau_R = \gamma/k = 18.85$ ms)(section 3.3.2). Besides, to use the strong friction approximation (neglect the inertia term), the time step should be larger than the momentum decay time τ_M. Therefore, to fulfill the above requirements, we made $\Delta t = 25$ µs. In Figure 3, the dependence of the position with time, for our simulation. The random number generator plays a crucial role, so we did the chi-squared test to verify the reliability of the random number generator of w_i (Figures 4 and 5).

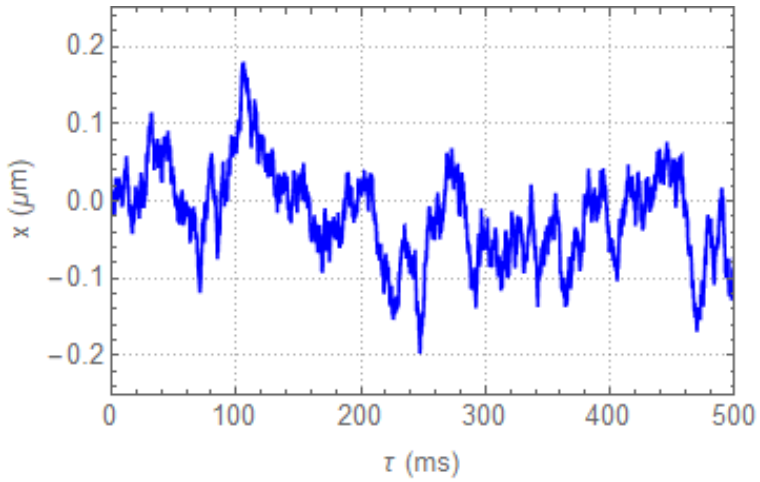

Figure 3 – Simulation of the motion of a free colloidal particle in water at temperature $T = 300$ K.

Source: By the author

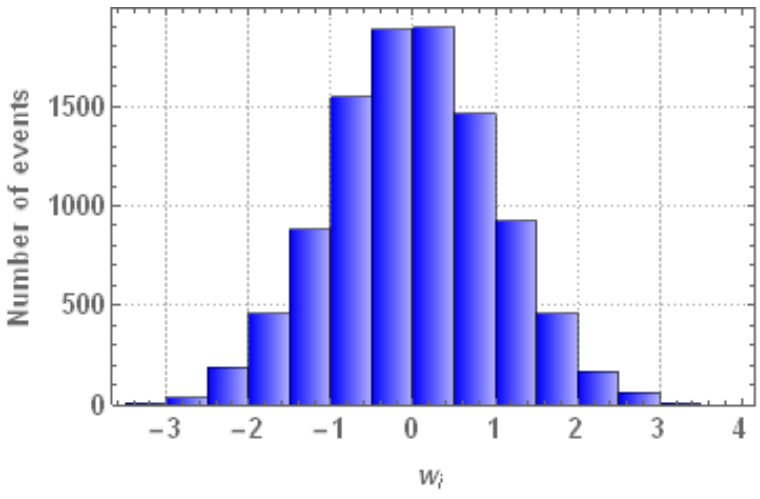

Figure 4 – Histogram constructed using 10000 realizations of w_i. The χ^2 of the distribution is $\chi^2 = 19.267$ with 13 degrees of freedom. Also, the average value is equal to 0.003 and standard deviation 1.010, as expected the properties of the white noise.

Source: By the author

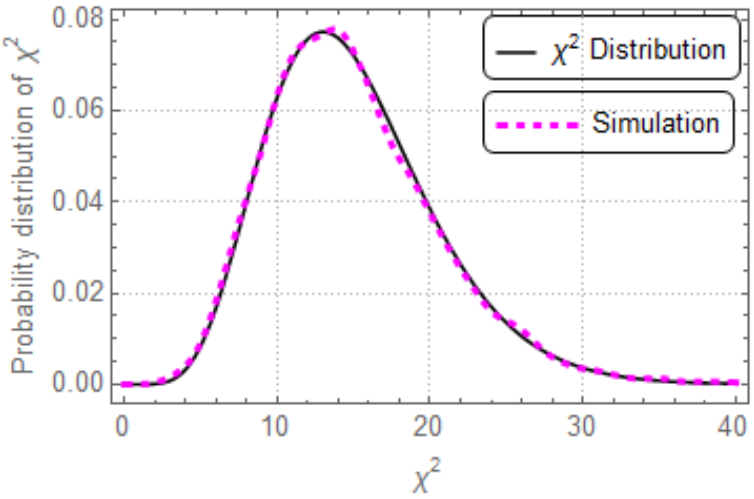

Figure 5 – χ^2 distribution. With the intent to verify if the random number generator is credible, we obtained the χ^2 value for 10000 trials (repeat the procedure in the Figure 4). Then, constructed its probability distribution (dashed/magenta). Note that it is in good agreement with the theoretical expectation (solid/black). Therefore, we can affirm that our random number generator have passed in the χ^2 test.

Source: By the author

3.3 The Fokker-Planck equation

Another manner of describing the system is by writing the time evolution of the probability distribution. In several situations, this description is more adequate than the one using the Langevin equation. Consider that $P(x,t)$ is the probability density function of the particle in the position x at time t. Then its time evolution is given by (see ref. (3) for a complete deduction)

$$\frac{\partial P(x,t)}{\partial t} = \frac{1}{\gamma}\frac{\partial}{\partial x}\left[\frac{dV(x)}{dx}P(x,t) + k_B T\frac{\partial P(x,t)}{\partial x}\right] \tag{3.23}$$

which is the Fokker-Planck equation in the strong friction limit. The probability satisfies the normalization condition

$$\int_{-\infty}^{\infty} P(x,t)dx = 1. \tag{3.24}$$

Now, let's explore the Fokker-Planck equation for two cases, the free particle and the harmonic potential.

3.3.1 Example 1: Free particle

For the free particle, the Fokker-Planck is written as

$$\frac{\partial P(x,t)}{\partial t} = \frac{k_B T}{\gamma}\frac{\partial^2 P(x,t)}{\partial x^2} \tag{3.25}$$

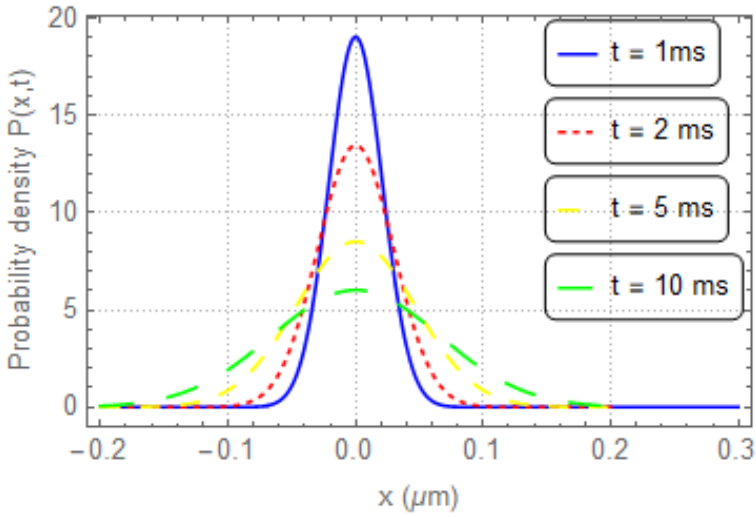

Figure 6 – Time evolution of the eq. (3.26), considering the initial probability density function $P(x,0) = \delta(x)$. As the time pass the probability distribution gets broader.

Source: By the author.

and is also known as the free diffusion equation. This equation can be solved using the Fourier transform. (35) If $P(x,0) = \delta(x)$, then the solution is

$$P(x,t) = \sqrt{\frac{\gamma}{4\pi k_B T t}} e^{\frac{-\gamma x^2}{4k_B T t}}. \tag{3.26}$$

Observe that the probability distribution is Gaussian. When time increases, the distribution becomes broader (Figure 6). Also, as the temperature increases the particle diffuses more quickly through the medium.

3.3.2 Example 2: Harmonic potential (Spectral Decomposition of the Fokker-Planck Equation)

The Fokker-Planck equation follows immediately and is given by

$$\frac{\partial P(x,t)}{\partial t_\gamma} = \frac{\partial}{\partial x}\left[\kappa x P(x,t) + k_B T \frac{\partial P(x,t)}{\partial x}\right], \tag{3.27}$$

where the adimensional factor $t_\gamma = t/\gamma$ is introduced. To solve the above partial differential equation, first, note that the operator

$$\hat{L}_{FP} = \kappa + \kappa x \frac{\partial}{\partial x} + k_B T \frac{\partial^2}{\partial x^2} \tag{3.28}$$

is not an self-adjoint operator. Nonetheless, there is a clever substitution that leads to one,

$$P(x,t_\gamma) = e^{-\gamma \kappa x^2/2g} \psi(x,t_\gamma). \tag{3.29}$$

With this substitution, the equation (3.27) becomes

$$\frac{1}{\kappa}\frac{\partial \psi(x,t_\gamma)}{\partial t_\gamma} = \left(\frac{1}{2} - \frac{\kappa x^2}{4k_B T}\right)\psi(x,t_\gamma) + \frac{k_B T}{\kappa}\frac{\partial^2 \psi(x,t_\gamma)}{\partial x^2}, \tag{3.30}$$

where the new operator

$$\hat{H}_{FP} = \frac{1}{2} - \frac{\kappa x^2}{4k_BT} + \frac{k_BT}{\kappa}\frac{\partial^2}{\partial x^2} \tag{3.31}$$

is self-adjoint. Therefore, the problem becomes a Sturm-Liouville problem and has well-known good properties.(35) In particular, it has eigenfunctions that form an orthonormal basis with real eigenvalues. The solution then may be written as a superposition of eigenfunctions of the problem. Accordingly, the solution for the initial probability density function $P(x,0) = \delta(x - x^{'})$ is equal to

$$P(x,t) = \sqrt{\frac{\kappa}{2\pi k_BT(1-e^{-2\kappa t/\gamma})}}\exp\left[\frac{-\kappa(x - x^{'}e^{-\kappa t/\gamma})^2}{2k_BT(1-e^{-2\kappa t/\gamma})}\right], \tag{3.32}$$

where $x^{'}$ is a constant. A validation test can be done by comparing the analytical solution of the probability distribution above with the probability distribution obtained for the simulations of the Langevin equation (Figure 7). The eq. (3.32) will be useful in calculating the dependence between the information-to-energy conversion and the delay time in section 6.4.5.

Note that, when $t \to \infty$ the probability density function turns into

$$P(x, t\to\infty) = \sqrt{\frac{\kappa}{2\pi k_BT}}\exp\left(\frac{-\kappa x^2}{2k_BT}\right), \tag{3.33}$$

that is the thermal distribution as expected from equilibrium Statistical Mechanics (see ref. (3)). The time scale for the system reach the thermal equilibrium state is determined by the relaxation time, defined as $\tau_R = \gamma/2\kappa$.

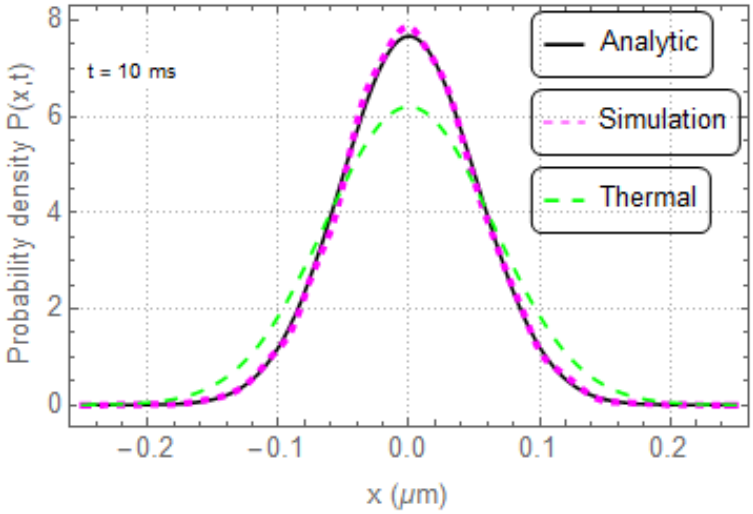

Figure 7 – Solution of the Fokker-Planck equation at 10 ms (solid/black), and the probability density function reconstructed from the Langevin equation using our simulation (dashed/magenta). They are in good agreement, showing again that the simulations are trustworthy. The tendency of both distributions is the state of thermal equilibrium (dashed/green), when $t \to \infty$.

Source: By the author.

4 STOCHASTIC ENERGETICS AND FLUCTUATION THEOREMS

In the previous chapter, we showed the theoretical foundation of this dissertation: the Langevin equation and the Fokker-Planck equation. However, thermodynamic work, heat, or entropy did not yet enter the stage.

In this chapter, we will show how to extend the concepts of classical thermodynamics to single trajectories of the Brownian particle. Also, we show that work becomes a stochastic quantity with its probability distribution respecting important relations as the Jarzysnki equality (JE) and the Crooks relation (CR). Because the Jarzysnki equality is an average over exponentials, it can be sensitive to rare events. We discuss the rare event's existence for a specific protocol and how the switching time affects the number of trials required for the convergence of the Jarzynski equality. For a quick review of the area, we refer to ref. (26)

4.1 Stochastic Energetics

Although classical thermodynamics typically deals with systems with myriads of degrees of freedom, Sekimoto showed in the late 90s that to each trajectory of a particle, quantities like work and heat can be associated, inaugurating what is known today as Stochastic energetics. (10) To see this, consider the Langevin equation (3.1) in the overdamped limit

$$-\frac{dV(x)}{dx} - \gamma\frac{dx(t)}{dt} + \sqrt{2k_BT\gamma}\xi(t) = 0. \tag{4.1}$$

Multiplying by $-dx$ (the multiplication in this context is the Stratonovich product, which is defined in such a manner that the chain rule of the ordinary calculus is still valid (33)) and rearranging, we obtain

$$-\left(-\gamma\frac{dx(t)}{dt} + \sqrt{2k_BT\gamma}\xi(t)\right)dx + \frac{dV(x)}{dx}dx = 0. \tag{4.2}$$

The first term describes the coupling between the particle and the bath and it is identified as heat dQ because it represents the energy dissipated in the medium. The second term is the internal energy change. Therefore, the equation can be rewritten as

$$dQ + dV = 0. \tag{4.3}$$

It is interesting to consider that, beyond the position, the potential energy can also depend on another parameter λ, called the work parameter (or control parameter). This is the variable that the experimentalist has control. Repeating the procedure above, we find

$$-\left(-\gamma\frac{dx(t)}{dt} + \sqrt{2k_BT\gamma}\xi(t)\right)dx + \frac{\partial V(x,\lambda)}{\partial x}dx = 0. \tag{4.4}$$

However, this time the last term does not represent the total energy change. For this, it is necessary to complete the differential form by adding to both sides the term $\frac{\partial V(x,\lambda)}{\partial \lambda} d\lambda$

$$dQ + dV = \frac{\partial V(x,\lambda)}{\partial \lambda} d\lambda. \tag{4.5}$$

The term of the right-hand side is identified as work dW, that is

$$dW = \frac{\partial V(x,\lambda)}{\partial \lambda} d\lambda \tag{4.6}$$

and we have an expression for the First Law of Thermodynamics for a single stochastic trajectory

$$dQ + dV = dW. \tag{4.7}$$

This new framework is called Stochastic Energetics. Note that $W > 0$ represents work delivered to the system. To obtain the work along a path, we integrated eq. (4.5) to get

$$W = \int_{\lambda_i}^{\lambda_f} \frac{\partial V(x,\lambda)}{\partial \lambda} d\lambda = \int_0^{\tau} \frac{d\lambda(t)}{dt} \frac{\partial V(x,\lambda)}{\partial \lambda} dt, \tag{4.8}$$

where λ_i and λ_f are the initial and final work parameter values, respectively. It is noteworthy that the work is positive ($W > 0$) when is delivered to the system and negative ($W < 0$) when the system does work. Alternatively, when we realize work on the system, $W > 0$, and when we receive work from the system, $W < 0$.

4.1.1 Control parameter and the breathing parabola

The acousto-optical modulator (chapter 2) allows controlling of the trap stiffness, κ, or of the trap center position, x_c, of the harmonic potential (eq. 2.1). The control of x_c is experimentally more difficult because it requires more calibrations. Therefore, we have focused on the control of the trap stiffness. Then, $\lambda = \kappa$, and the potential becomes,

$$V(x,\lambda) = \frac{\lambda x^2}{2} \tag{4.9}$$

where we chose $x_c = 0$. This is a paradigmatic case in stochastic thermodynamics known as the harmonic potential with time-dependent trap stiffness or the breathing parabola.

4.1.2 Protocols

The different manners to vary the work parameter, $\lambda(t)$, are called protocols (Figure (8)). The protocol duration, τ, is called protocol time or switching time. A convenient way to write $\lambda(t)$ is

$$\lambda(t) = \lambda_i + (\lambda_f - \lambda_i) g(s), \tag{4.10}$$

where $s = t/\tau$. The function $g(s)$ is also known as a protocol and satisfies the conditions $g(0) = 0$ and $g(1) = 1$.

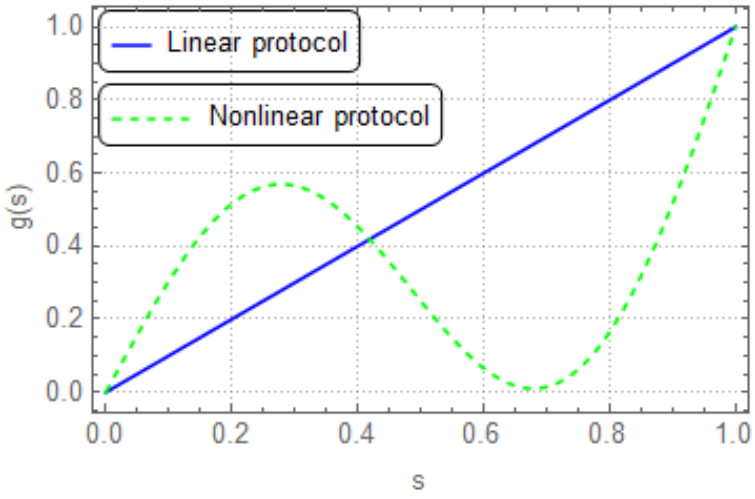

Figure 8 – Example of protocols. The work parameter can increase linearly (solid/blue) or have a non-linear behaviour (dashed/green).

Source: By the author.

4.1.3 Average work

Because the stochastic work fluctuates, a more interesting quantity is the average work $\langle W \rangle$. It is defined as the work averaged over all stochastic realizations (over the thermal distribution and over the noise), and using eq. (4.8) can be written as

$$\langle W \rangle = \int_0^\tau \frac{d\lambda(t)}{dt} \left\langle \frac{\partial V(x,\lambda)}{\partial \lambda} \right\rangle dt, \tag{4.11}$$

where the bracket, $\langle \cdot \rangle$, represents the average over all realizations. Another way to represent the average work is through

$$\langle W \rangle = \int P(W) W dW, \tag{4.12}$$

with $P(W)$ representing the work probability density function (Figure 9). Different protocols generate different probabilities distributions and average values for the work.

4.1.4 Helmholtz free energy

The Helmholtz free energy, F, is a helpful quantity in classical thermodynamics in treating systems in contact with a thermal reservoir. In this context, the Helmholtz free energy difference, ΔF, is equal to the work given to the system to reversibly change between equilibrium states while in contact with a thermal reservoir. (2) However, if the process is irreversible, then

$$\Delta F \leq W_{classical} \tag{4.13}$$

which is equivalent to the Second Law of Thermodynamics. Even though the stochastic work fluctuates, its average value is still larger than the free energy difference, i.e.

$$\Delta F \leq \langle W \rangle. \tag{4.14}$$

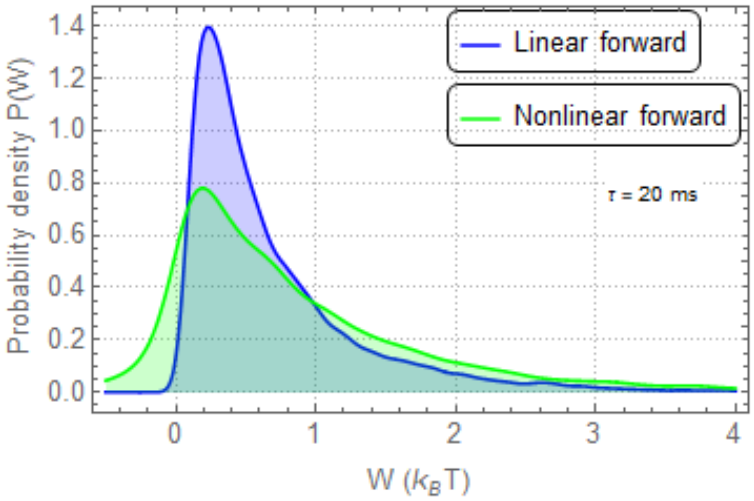

Figure 9 – Work probability density function, $P(W)$, for the protocols given in Figure 8. Although the probability density functions are different with distinct average values, both respect the Jarzynski equality (eq. (4.41)).

Source: By the author.

In the limit of an infinitely long process ($\tau \to \infty$), the protocol is so slow that the system remains in thermal equilibrium at all times. Thus, the process is reversible, and we retrieve

$$\langle W \rangle = \Delta F. \tag{4.15}$$

Statistical mechanics provides an expression for the Helmholtz free energy. So,

$$F(\lambda) = -k_B T \ln Z = -k_B T \ln \int \exp(-V(\Gamma, \lambda)/k_B T) d\Gamma, \tag{4.16}$$

where

$$Z = \int \exp(-V(\Gamma, \lambda)/k_B T) d\Gamma \tag{4.17}$$

is the partition function, and Γ is a point in the phase space. For the harmonic potential with time-dependent stiffness, the free energy difference is given by

$$\Delta F(\lambda) = k_B T \ln \left(\frac{\lambda_f}{\lambda_i} \right), \tag{4.18}$$

where we use eqs. (4.9) and (4.16).

4.1.5 Example: Instantaneous protocol

Consider the harmonic potential with time dependent stiffness. An important protocol is the immediate jump (or instantaneous protocol). The trap stiffness changes, instantaneously, from λ_i to λ_f. Therefore, $\tau = 0$. Using eqs. (4.6) and (4.9), the stochastic work is written as

$$dW = \frac{x^2}{2} d\lambda \tag{4.19}$$

Integrating the equation above, we obtain

$$W = \frac{x^2}{2}\Delta\lambda, \tag{4.20}$$

where $\Delta\lambda = \lambda_f - \lambda_i$. Note that the work for an instantaneous protocol is equal to the difference of the final and initial potentials, i.e., $W = V(x, \lambda_f) - V(x, \lambda_i)$.The average work then becomes

$$\langle W \rangle = \frac{\Delta\lambda}{2}\langle x^2 \rangle. \tag{4.21}$$

Since the protocol is instantaneous, the average $\langle x^2 \rangle$ is over the probability distribution of x at the beginning of the protocol, i.e.,

$$\langle x^2 \rangle = \int_{-\infty}^{\infty} x^2 P(x, 0) dx, \tag{4.22}$$

where $P(x, 0)$ is the initial probability density function. If, initially, the particle is in thermal equilibrium, then

$$P(x, 0) = \sqrt{\frac{\lambda_i}{2\pi k_B T}} \exp\left(\frac{-\lambda_i x^2}{2k_B T}\right). \tag{4.23}$$

Substituting eq.(4.23) into eq. (4.22), we obtain

$$\langle x^2 \rangle = \frac{k_B T}{\lambda_i}. \tag{4.24}$$

Therefore, using eqs. (4.21) and (4.24),the average work is equal to

$$\frac{\langle W \rangle}{k_B T} = \frac{1}{2}\left(\frac{\lambda_f}{\lambda_i} - 1\right). \tag{4.25}$$

4.1.6 Example: Linear protocol

Another important example is the linear protocol. The work parameter is changed from λ_i to λ_f is a time τ, at a constant rate. The protocol can be written either as,

$$\lambda(t) = \lambda_i + \frac{\Delta\lambda}{\tau}t \tag{4.26}$$

or as

$$g(s) = s = \frac{t}{\tau}. \tag{4.27}$$

The average work can be calculated using eqs. (4.11), (4.9), and (4.26). Thus,

$$\langle W \rangle = \frac{\Delta\lambda}{2\tau}\int_0^{\tau} \langle x^2 \rangle dt. \tag{4.28}$$

In the previous example, we needed to know the quantity $\langle x^2 \rangle$ at the beginning of the protocol to evaluate the average work. However, in this example, because $\langle x^2 \rangle$ is integrated in time, we need its time evolution during the protocol. Two paths can be taken to obtain the time dependence of $\langle x^2 \rangle$.

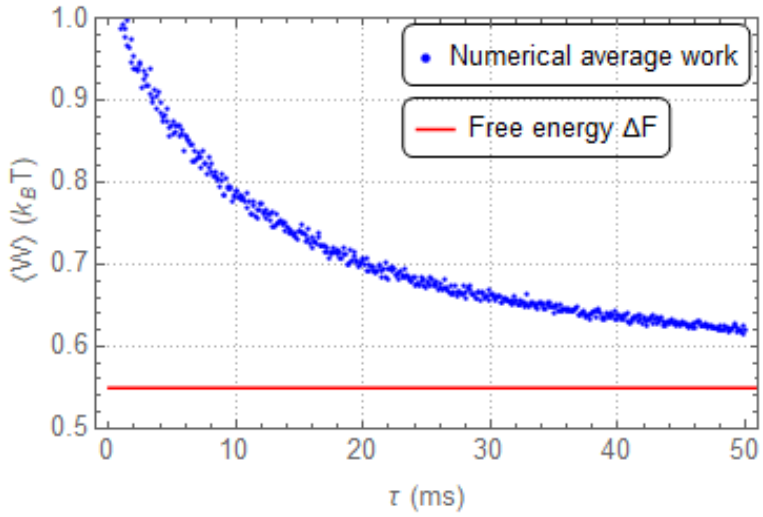

Figure 10 – As expected, in the overdamped regime the mean value of work for a linear protocol (blue/dots) decays to its free energy difference (solid/red) monotonically, as the switching time increases.

Source: By the author.

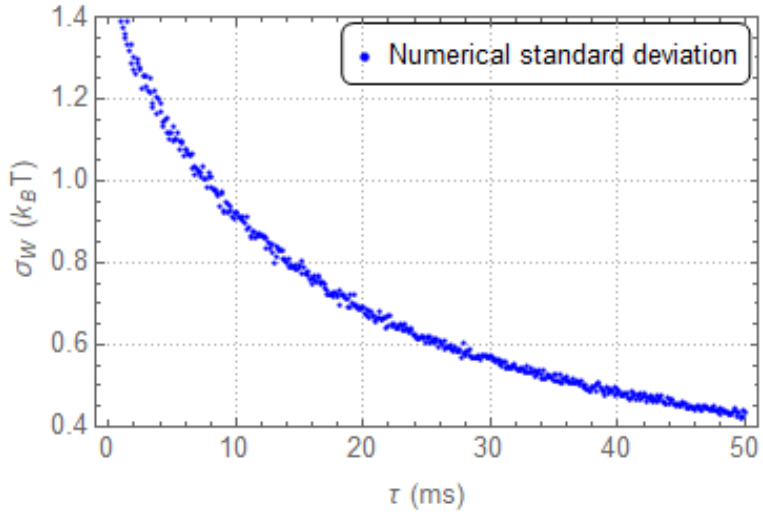

Figure 11 – The standard deviation for a linear protocol decreases monotonically to zero as the switching time increases.

Source: By the author.

First, the time evolution of $\langle x^2 \rangle$ can be obtained by simulating the Langevin dynamics. In Figures (10) and (11) are our results for the simulations of the Langevin equation for the linear protocol. It is noteworthy that the work decays to the free energy difference while the standard deviation goes to zero. However, we do not have to simulate the Brownian motion of the microparticle to obtain $\langle W \rangle$.

Alternatively, $\langle x^2 \rangle$ can be obtained by multiplying the Fokker-Planck equation

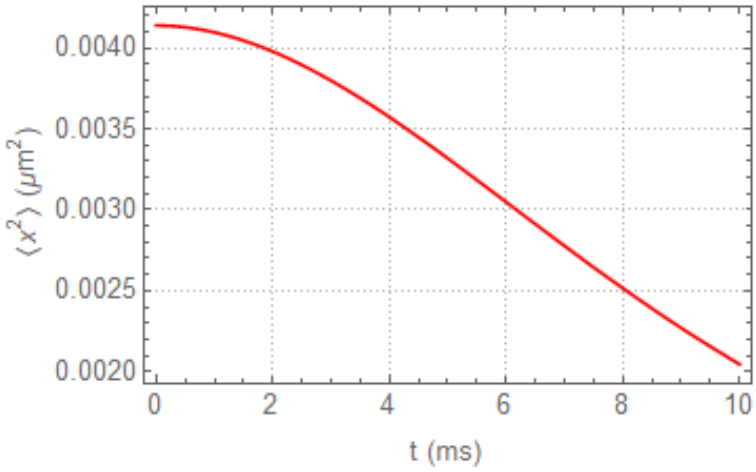

Figure 12 – Evolution of $\langle x^2 \rangle$ during the linear protocol, obtained numerically using eq. (4.29). Initially, the particle is at thermal equilibrium and the protocol time is equal to $\tau = 10$ ms. By integrating such curve, we obtain an average work equal to $\langle W \rangle = 0.785\ \mathrm{k_B T}$.

Source: By the author

(3.23) by x^2 and integrating it. Defining $w(t) = \langle x^2 \rangle$, the time evolution is written as

$$\frac{dw}{dt} = -\frac{2\lambda}{\gamma} w + \frac{2k_B T}{\gamma}. \tag{4.29}$$

This equation can be numerically solved given an initial condition $w(0)$ (Figure 12). With the solution and eq. (4.28), the average work is obtained.

4.1.7 Observation: alternative identification of the work

One could think that the work expression is rather odd or even wrong since apparently, it does not agree with the more traditional view of work being equal to force times displacement. Villar and Rubi (36) used this apparent inconsistency between definitions to criticize the work identification using eq. (4.11). Soon after, rebuttals to this criticism were published. (37–39) Nonetheless, an alternative identification (which agrees with the conventional view) of the work is possible in the framework developed. However, in the quasistatic limit, the alternative identification does not tend to the free energy difference, as expected from classical thermodynamics. Therefore, the more used definition for the work in the literature is of eq. (4.11), and it is the definition that we use in this dissertation.

4.2 Entropy and the Second Law of Thermodynamics

The last thermodynamic quantity that we introduce is the entropy. As the work, the entropy production allows more than one identification. The different definitions have different features, like the existence of negative entropy production rates. (40) The two

distinct entropy production identifications that we will discuss in this section are the informational entropy (6) and the irreversible work entropy. (40) For a more detailed discussion we refer to ref. (41).

4.2.1 Informational entropy

Following refs. (6, 8), it seems natural to associate a contribution to the entropy production, $\Delta\Sigma_m$, from the heat dissipated in the medium

$$\Delta\Sigma_m = \frac{Q}{T}. \tag{4.30}$$

Besides, a trajectory dependent entropy, $\sigma(t)$, can be identified. Using the Shannon entropy (ref. (42)),

$$\Sigma(t) = \langle\sigma(t)\rangle = -\int P(x(t),t)\ln P(x(t),t)dx, \tag{4.31}$$

one defines the stochastic entropy as

$$\sigma(t) = -\ln P(x(t),t), \tag{4.32}$$

where $P(x(t),t)$ is the solution of the Fokker-Planck equation (3.23) evaluated along the trajectory $x(t)$. Note that the probability of a trajectory depends on the initial ensemble. Therefore, even if we have two equal trajectories, its probability to happen can be different, if the initial probabilities distributions are different. If the particle is initially at thermal equilibrium, then the probability density function is given by the Gibbs distribution

$$P(x(0),0) = \frac{\exp\left[-\frac{V(x(0),0)}{k_BT}\right]}{Z}, \tag{4.33}$$

where

$$Z = \int \exp\left[-\frac{V(x(0),0)}{k_BT}\right] dx \tag{4.34}$$

is the partition function. Substituting eqs. (4.33) and (4.34) in (4.32), we obtain the relation

$$T\sigma(x(t)) = V(x(t),t) - F. \tag{4.35}$$

4.2.2 Irreversible work

Another possible identification for the entropy production is given in ref. (40). If $\Delta\Sigma_S$ is the entropy production of an isolated system, $\Delta\Sigma_B$ the entropy production of the heat bath, then the total entropy production, $\Delta\Sigma_{tot}$, is equal to

$$\Delta\Sigma_{tot} = \Delta\Sigma_S + \Delta\Sigma_B. \tag{4.36}$$

Using the Clausius theorem and the the First Law of Thermodynamics, the above expression can be written as

$$T\Delta\Sigma_{tot} = T\Delta\Sigma_S + \langle W\rangle - \Delta V. \tag{4.37}$$

Substituting the expression $\Delta F = -T\Delta\Sigma_S + \Delta V$, we obtain

$$T\Delta\Sigma_{tot} = \langle W \rangle - \Delta F. \tag{4.38}$$

However, the irreversible work, $\langle W_{irr} \rangle$, is defined as

$$\langle W_{irr} \rangle = \langle W \rangle - \Delta F. \tag{4.39}$$

Therefore,

$$T\Delta\Sigma_{tot} = \langle W_{irr} \rangle \tag{4.40}$$

and the irreversible work can be used as a measure of the entropy production.

4.3 Fluctuation Theorems

4.3.1 Jarzysnki equality

We have seen that work fluctuates in each realization, with its values being distributed according to a probability density function $P(W)$. Christopher Jarzysnki showed in 1997 (43), that

$$\langle \exp(-W/k_BT) \rangle = \exp(-\Delta F/k_BT) \tag{4.41}$$

if, initially, the particle is in thermal equilibrium. This relation gives a connection between two equilibrium states with a non-equilibrium quantity. Due to the concavity of the exponential function, it is easy to recover

$$\Delta F \leq \langle W \rangle, \tag{4.42}$$

as expected.

The Jarzysnki equality has various applications, mainly in estimating free energy differences. However, in our case, we already have an analytical expression for the free energy difference (eq. (4.18)), and therefore, we use JE as a test for our simulations.

A practical question that often arises is how many realizations are necessary for the convergence of the Jarzynski equality, as discussed in refs. (44) and (45). Because of the fluctuating work, some values are dominant in the average process, i.e., some values of W will contribute more than others in the average $\langle \exp(-W/k_BT) \rangle$. Note that dominant work values arise from two factors: the weight $\exp(-W/k_BT)$ and the probability of the event to occur. For example, a work value can be a frequent event, yet its weight can be tiny, leading to a small contribution to the average $\langle \exp(-W/k_BT) \rangle$. Furthermore, a work value can be rare with a large weight, resulting in an important contribution to the convergence of JE. In the experiment, the number of realizations must be enough to see a few of the dominant values to guarantee the convergence of JE. If the dominant values are rare, then more realizations of the experiment are necessary. Typically, in our simulations,

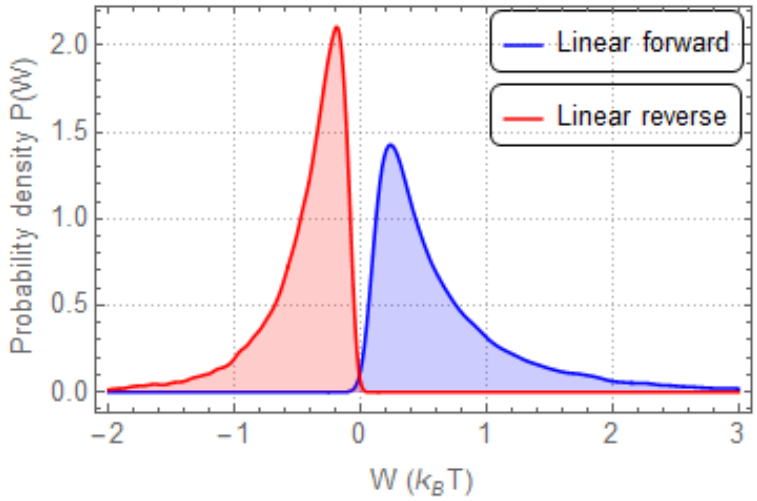

Figure 13 – Probability density functions for the forward linear protocol, $P(W)$, and for the reverse, $P^{\dagger}(W)$. This two distributions allows one to verify the Crooks relation (eq. (4.43)).

Source: By the author.

10000 realizations are made for a given set of parameters (protocol time, initial and final work parameters, temperature, etc.). We are going to justify such a number in section 4.4.

Although JE was first derived using Hamiltonian dynamics, soon after, the result was extended for stochastic dynamics, see ref. (5)

4.3.2 Crooks relation

A refinement of the Jarzynski equality is the Crooks relation. (6) This relation connects the work distribution for a protocol in the forward direction with its reverse. The relation reads

$$P(W)/P^{\dagger}(-W) = \exp[(W - \Delta F)/k_B T], \tag{4.43}$$

where $P^{\dagger}(W)$ is the probability density function for the reverse protocol (as shown in Figure 13). The reverse protocol $\lambda^{\dagger}(t)$ is defined as

$$\lambda^{\dagger}(t) = \lambda(\tau - t). \tag{4.44}$$

A comparison of the Crooks relation for the simulation is in Figure (14).

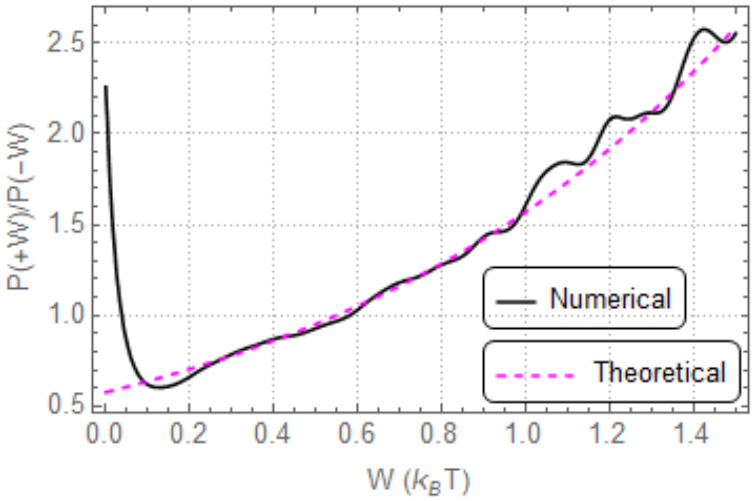

Figure 14 – Comparison of the Crooks relation between theoretical and numerical data for a linear protocol. In magenta/dashed is eq. (4.43) and in black/solid the result of the simulation. Due to the finite number of realizations, the simulated result diverges from the theoretical result for more rare work values. But, they are in good agreement in the central region.

Source: By the author.

4.4 Role of the rare events and the number of realizations

The Jarzynski equality, as we mentioned, is a useful relation in checking the validity of our simulations. However, it is an average value. Thus, the experiment must be performed several times to see this average convergence. The so-called dominant work values are the events that have a crucial role in the JE convergence. They can be rare events, and, in consequence, the number of realizations to converge can be large. Here, we use the knowledge of the work distribution to investigate the dominant work values, their probability, and the dependence on the protocol time.

4.4.1 Linear forward protocol

To study the number of realizations needed for convergence, note that the quantity $\langle \exp(-W/k_BT) \rangle$ can be written as

$$\langle \exp(-W/k_BT) \rangle = \int \exp(-W/k_BT) P(W) dW. \tag{4.45}$$

Thus, the area under curve $\exp(-W/k_BT)P(W)$ gives the left-hand side of JE. The idea is to obtain the probability density function, $P(W)$, and consequently $\exp(-W/k_BT)P(W)$. Then, see the values of W in which $\exp(-W/k_BT)P(W)$ has the larger values because these are the work values that contribute the most, i.e., the dominant work values. Next, we look at the probability of such events to occur. If the probability is low, the event is rare, and it is necessary to perform the experiment several times.

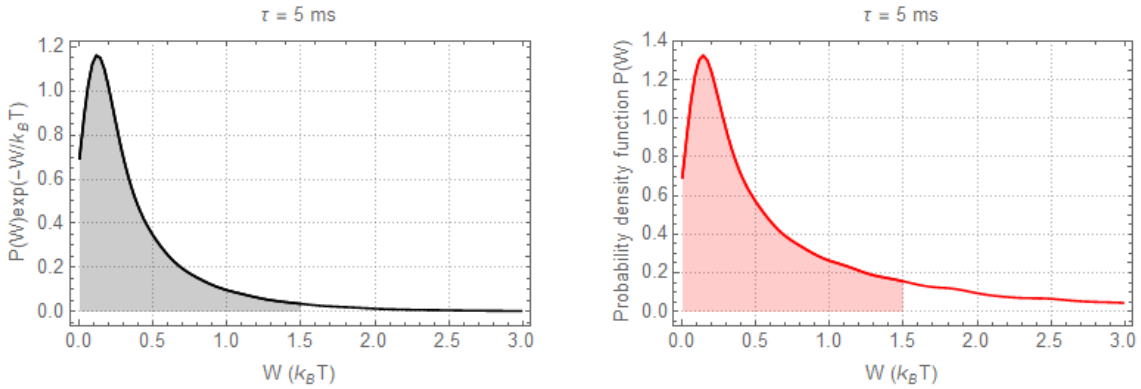

(a) (b)

Figure 15 – (a) $P(W)\exp(-W/k_BT)$. The total area (highlighted and not highlighted) gives $\langle\exp(-W/k_BT)\rangle$. The black area represents the work values that contribute the most to JE convergence. In other words, the highlighted area represents the dominant work values. The interval goes from 0 to the average of the distribution plus three standard deviations of the same curve. (b) Probability density function, $P(W)$, for a linear protocol of 5 ms. The red highlighted area represents the probability of occurrence of the dominant work values determined previously.

Source: By the author.

Figure 15 shows an example of the previous reasoning for a linear protocol. Since the protocol increases monotonically, there are only positive values for the work. Thus, small values of work have large values of $\exp(-W/k_BT)P(W)$. Nonetheless, they also have a high probability to happen. Therefore, for the forward linear protocol, there are no rare events, and a small number of realizations guarantee convergence (as shown in Figure 16).

We highlight that the values of W that are important to the convergence come from a balance between probability and work value. Negative W values have a great weight, but they will contribute only if their probability of occurrence is considerable.

4.4.2 Number of realizations and the protocol time

In estimating the probability of dominant work values to occur, we rely on the probability density function, $P(W)$. This distribution changes if the protocol time is different. Thus, we repeat the procedure described in the previous section for the linear protocol for distinct switching times (as shown in Figure 17). When the protocol is slow, the distribution tends to a Gaussian and becomes narrower. (46) Then, the number of necessary realizations decreases as the protocol time increases due to the narrower work distribution. For rapid protocols, the work distribution is broader, leading to a large number of realizations for convergence.

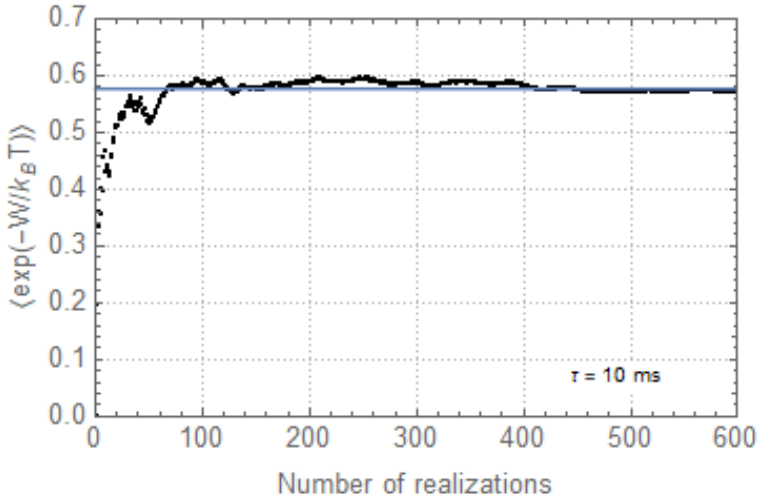

Figure 16 – Convergence of $\langle \exp(-W/k_BT) \rangle$ (black/dots). The larger the number of realizations, the closer the average becomes to $\exp(-\Delta F/k_BT)$(blue/solid). It is noteworthy that the lack of rare events causes the quick convergence of the JE (approximately 500 realizations). Therefore, justifying the 10000 realizations performed in simulations.

Source: By the author.

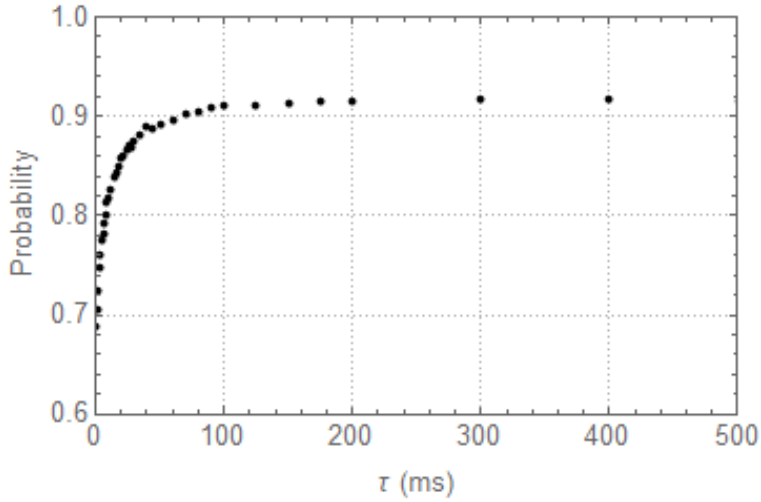

Figure 17 – Protocol time and probability to obtain a dominant work value. As we increase the former, the latter also increases.

Source: By the author.

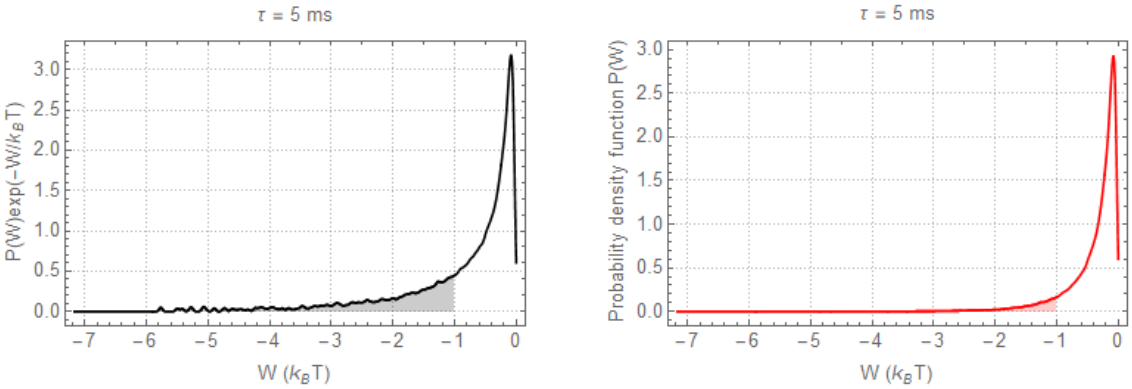

(a) (b)

Figure 18 – (a) The highlighted area has a significant contribution to the integral (eq. (4.45)). (b) Probability density function, $P^{\dagger}(W)$, for a linear reverse protocol. The highlighted area represents work values that contribute to the JE convergence. Nonetheless, it has a small probability of occurrence.

Source: By the author.

4.4.3 Reverse linear protocol

In the previous example, we saw that the linear protocol generated only positive values for the stochastic work. However, in section 6.3.1, when studying feedback control, the presence of negative values of work will increase the number of realizations necessary to the convergence of the Generalized Jarzynski equality. Therefore, we will treat an example that has negative values of work.

The reverse linear protocol only has negative values of the stochastic work. The analysis utilized for the forwad linear protocol is not appropriate in this case. Because the probability density function $P(W)$ is narrower than $P(W)\exp(-W/k_BT)$, the procedure presented in the previous section fails. If we apply the method here, the result would be that the probability of a dominant event happening is close to 1, i.e., all events are dominant. Nonetheless, the number of realizations is not small since there are dominant W values with a small probability of occurrence. The analysis made is in Figure 18.

Figure 18-a shows that highlighted area has a considerable contribution to $\langle\exp(-W/k_BT)\rangle$. However, it has a tiny probability of occurrence, as shown in 18-b. Therefore, these events are rare dominant W values, and a large number of realizations are necessary.

In contrast, in the previous example the highlighted area in Figure 15-a also has a considerable contribution to $\langle\exp(-W/k_BT)\rangle$ but with a high probability of happening. So, the dominant events are frequent and a small number of realizations are necessary.

5 OPTIMAL PROTOCOLS

In the last chapter, we saw that finite-time processes requires work, where its average is always larger than the Helmholtz free energy difference between the final and initial states of the system. In this context, optimal protocols minimize the irreversible work and, generally, they are hard to find analytically. However, paradigmatic examples, as the harmonic potentials with time-dependent center position and time-dependent stiffness, have analytic solutions in the overdamped regime, which we will explore here. These solutions present counter-intuitive features, like jumps and delta-peaks, at the beginning and end of the protocols. (15, 47)

In this chapter, we begin by reviewing the exact optimal protocol in the overdamped regime for the breathing parabola. (15) The exact optimal protocol gives a reference average work value that can be compared with the value delivered by other methods to verify the closeness of the protocols produced.

The first alternative method to find the optimal protocol studied was for slowly varying processes. (17, 48) Slowly varying processes are processes that are slow but not necessarily weak. Alternatively, we also studied a phenomenological linear response theory method described in ref. (18) This method does not require knowledge about the microscopic properties of the system, simplifying the treatment of other cases. It is a phenomenological method because it uses the relaxation function, which can be measured in the laboratory.

The performance of the protocols generated with the previous approximate methods has not been explored numerically in the literature. Here, our main result is the determination of the performance of the methods for different protocol times and changes of the control parameter. We show that the performance of the phenomenological method is good even outside its theoretical validity regime.

5.1 Exact optimal protocols

In ref. (15) Schmiedl and Seifert have deduced the optimal protocols for the harmonic potential with time-dependent trap's center position and stiffness. As already said, we are mostly interested in this dissertation in the breathing parabola. Thus, using eqs. (4.8) and (4.9) , we write the work as

$$\langle W \rangle = \frac{1}{2}\int_0^\tau \frac{d\lambda}{dt}\langle x^2 \rangle dt = \frac{1}{2}\int_0^\tau \frac{d\lambda}{dt} w(t) dt, \tag{5.1}$$

where $w(t) = \langle x^2 \rangle$. The time evolution of $w(t)$ can be obtained from the Fokker-Planck (as done in section 4.1.6),

$$\frac{dw}{dt} = -\frac{2\lambda}{\gamma} w + \frac{2k_B T}{\gamma}, \tag{5.2}$$

where the differential equation can be solved given an initial condition $w(0)$. Integrating by parts equation (5.1), we obtain

$$\langle W \rangle = \frac{1}{2} \left(\lambda(t) w(t) \Big|_0^\tau - \int_0^\tau \lambda \frac{dw(t)}{dt} dt \right). \tag{5.3}$$

Isolating λ from equation (5.2) and substituting in the above equation, we rewrite eq. (5.3) as

$$\langle W \rangle = \frac{1}{2} (w(t)\lambda(t) - k_B T \ln w(t)) \Big|_0^\tau + \frac{\gamma}{4} \int_0^\tau \frac{1}{w} \left(\frac{dw}{dt} \right)^2 dt. \tag{5.4}$$

First, we minimize the integral on the right-hand side. The minimization of the work functional corresponds to solving the Euler-Lagrange equation (35)

$$\left(\frac{dw}{dt} \right)^2 - 2w \frac{d^2 w}{dt^2} = 0. \tag{5.5}$$

The solution is equal to

$$w(t) = c_1 (1 + c_2 t)^2. \tag{5.6}$$

where c_1 and c_2 are constants. If, initially, the particle is in thermal equilibirum, then $w(0) = \frac{k_B T}{\lambda_i}$, fixing the constant c_1. The second constant, c_2, we find by minimizing the total work

$$\langle W \rangle = \frac{\lambda_f}{2\lambda_i} (1 + \tau c_2)^2 + \frac{(\tau c_2)^2 \gamma}{\lambda_i \tau} - \frac{1}{2} - \ln(1 + c_2 \tau). \tag{5.7}$$

The value of c_2 that minimizes the above expression is equal to

$$c_2 \tau = \frac{-\gamma - \tau \lambda_f + \sqrt{\gamma^2 + 2\gamma\tau\lambda_i + \tau^2 \lambda_f \lambda_i}}{2\gamma + \lambda_f \tau}. \tag{5.8}$$

Using equations (5.2), (5.6), and (5.8), we get the optimal protocol for the time-dependent stiffness of a harmonic potential

$$\lambda(t) = \frac{\lambda_i - \gamma c_2 (1 + c_2 t)}{(1 + c_2 t)^2}. \tag{5.9}$$

If, we substitute $t = 0$ in the above equation, we obtain

$$\lambda(0) = \lambda_i - \gamma c_2 \neq \lambda_i. \tag{5.10}$$

Therefore, the protocol has a discontinuity/jump at the beginning of the protocol. The same happens for $t = \tau$, i.e., $\lambda(\tau) \neq \lambda_f$. The analysis of eqs. (5.7) and (5.9) is on Figure (19).

A larger variation of the work parameter leads to a more accentuated concavity of the protocol (Figure 19-a). The explanation relies upon considering that the larger the work parameter, the more rapidly the system tends to equilibrium (section 3.3.2). Therefore, when the work parameter is large, it can quickly change without getting far from equilibrium.

5.1.1 Limiting cases

As a verification of expression (5.7), we can make the protocol time arbitrarily short or long. For rapid protocols, we have

$$\lim_{\tau \to 0} c_2 \tau \to 0, \tag{5.11}$$

and

$$\langle W \rangle \to \frac{1}{2} \left(\frac{\lambda_f}{\lambda_i} - 1 \right), \tag{5.12}$$

which is equal to the average work of the instantaneous protocol (section 4.1.5), as expected. For arbitrarily long protocols,

$$\lim_{\tau \to \infty} c_2 \tau \to \left(\sqrt{\frac{\lambda_f}{\lambda_i}} - 1 \right), \tag{5.13}$$

and

$$\langle W \rangle \to \Delta F. \tag{5.14}$$

So, the average work in the quasistatic limit is equal to the free energy difference of the system (section 4.1.4).

5.1.2 Performance

Eqs. (5.7) and (5.8) give the minimum average work required to change the work parameter from λ_i to λ_f in a finite-time for the breathing parabola. In more general cases, the work functional may not be so simple, justifying the necessity of other methods. To compare the different methods with the developed in this section, we define the performance of a protocol as the relative difference between the average work given by a certain method, $\langle W_{aprox.} \rangle$, and the exact value given by eq. (5.7), i.e.,

$$\text{Performance} = \frac{\langle W_{aprox.} \rangle - \langle W_{exact} \rangle}{\langle W_{exact} \rangle}. \tag{5.15}$$

We say that a method has a good performance when the value of the relative difference above is small.

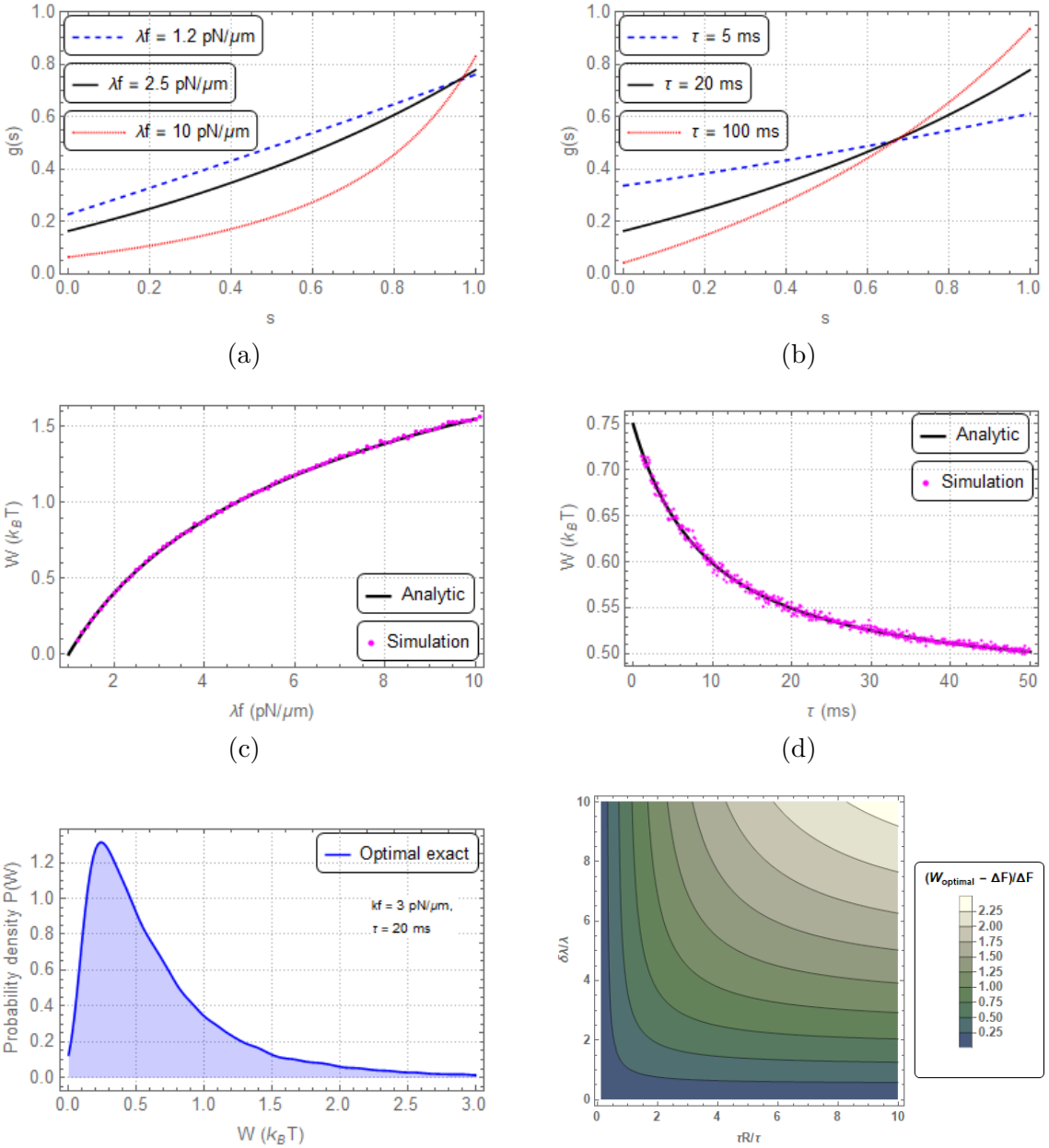

Figure 19 – (a) Relation between the exact optimal protocol (eq. (5.9)) and the final work parameter, λ_f. The switching time is equal to $\tau = 20$ ms. Note the discontinuities at the beginning and end of the protocols. Remember that $g(0) = 0$ and $g(1) = 1$ (eq. (4.10)). So, the optimal protocols have jumps in the extremities. (b) For $\lambda_f = 2.5$ pN/μm, how the optimal protocol (eq. (5.9)) varies with the switching time. The faster the protocols, the greater is the discontinuity. (c)(d) The optimized work (eq. (5.7)) increases as we increase λ_f and decreases when we increase the switching time, τ. The work returned by the simulation (dots/magenta) of the optimal protocol (5.7) and the theoretical expectation (solid/black). We see that they are in good agreement. (e) A work distribution for the optimal protocol. (f) A map of the relative difference between the minimum work (eq. (5.7)) and the free energy difference (eq. (4.18)). It gives a raw estimative of what are nonequilibrium processes.

Source: By the author.

5.2 Optimal protocols for slowly varying process

Linear response theory is valid in a regime in which the control parameter has only small variations, i.e., it is the regime of weak protocols ($\Delta\lambda/\lambda_i \ll 1$). It infers non-equilibrium quantities from equilibrium measurements. Slowly varying processes are protocols that are slowly driven but, they are not necessarily weak. For both regimes, linear response theory or slowly varying processes, the systems stay close to equilibrium. Note that for the former regime, because the work parameter variation is small, the system stays close to equilibrium even if it is driven quickly. On the other side, slowly varying processes remain close to equilibrium because the system changes very slowly. Therefore, it has enough time to relax back to equilibrium. Thus, the switching time must be much larger than the relaxation time of the system.

In the linear response regime ($\Delta\lambda/\lambda_i \ll 1$), we can write the Hamiltonian of the system as

$$H[\lambda(t)] = H(\lambda_i) + \Delta\lambda g(t)\frac{\partial H}{\partial \lambda} + \mathcal{O}(\Delta\lambda^2), \tag{5.16}$$

where we are treating the hamiltonian perturbatively. The expression for the work (eq. (4.11)), is given in term of the Hamiltonian as

$$\langle W \rangle = \int_0^\tau \frac{d\lambda(t)}{dt}\left\langle \frac{\partial H}{\partial \lambda}\right\rangle dt. \tag{5.17}$$

Then, by using some linear response theory methods (4), we get the expression for the non-equilibrium average

$$\left\langle \frac{\partial H}{\partial \lambda}\right\rangle = \left\langle \frac{\partial H}{\partial \lambda}\right\rangle_{eq;\lambda_i} + \chi_0^\infty \Delta\lambda g(t) - \Delta\lambda \int_0^t ds \phi_0(t-s)g(s), \tag{5.18}$$

where $\langle\ \cdot\ \rangle_{eq;\lambda_i}$ is the average over the equilibrium state with work parameter λ_i. The second term on the right-hand side describes the instantaneous response

$$\chi_0^\infty = \left\langle \frac{\partial^2 H}{\partial \lambda^2}\right\rangle_{eq;\lambda_i}, \tag{5.19}$$

while the last term is the delayed response. The function $\phi_0(t)$ is the response function, equal to

$$\phi_0(t) = \langle \{X(0), X(t)\}\rangle_{eq;\lambda_i} \tag{5.20}$$

where $\{\ \cdot\ \}$ is the Poisson bracket and

$$X = \frac{\partial H}{\partial \lambda} \tag{5.21}$$

is known as generalized force. Employing Kubo's formula obtain

$$\Psi(t) = \beta(\langle X(0)X(t)\rangle_{eq;\lambda_i} - \langle X(0)\rangle^2_{eq;\lambda_i}), \tag{5.22}$$

where $\Psi_0(t)$ is the relaxation function. Therefore, eq. (5.18) can be re-written after an integration by parts as

$$\left\langle \frac{\partial H}{\partial \lambda} \right\rangle = \left\langle \frac{\partial H}{\partial \lambda} \right\rangle_{eq;\lambda_i} - \tilde{\Psi}\Delta\lambda g(t) + \Delta\lambda \int_0^t ds \Psi(u) \frac{dg}{dt'}\bigg|_{t'=t-u} \tag{5.23}$$

where $\tilde{\Psi} = \Psi(0) - \chi_0^\infty$. For applying this to slowly varying processes, the idea is to break the protocol in several steps, small enough that in each one we can apply linear response theory. The result for the irreversible work (eq. (4.39)) is equal to

$$\langle W_{irr} \rangle = \frac{\beta(\Delta\lambda)^2}{\tau} \int_0^1 ds \left(\frac{dg}{ds}\right)^2 \tau_R[g(s)]\chi[g(s)] \tag{5.24}$$

where

$$\tau_R[\lambda(t)] = \int_0^\infty du \frac{\Psi_0(u)}{\Psi_0(0)} \tag{5.25}$$

is the relaxation (or correlation) time in linear response theory and determines the time scale over which the response vanishes, i.e., the system relaxes back to equilibrium. $\chi[\lambda(t)]$ is defined by

$$\chi[\lambda(t)] = \left\langle \left(\frac{\partial H}{\partial \lambda}\right)^2 \right\rangle_{eq;\lambda} - \left\langle \frac{\partial H}{\partial \lambda} \right\rangle^2_{eq;\lambda}. \tag{5.26}$$

Thus, the method consists in using eqs. (5.22), (5.21), (5.25) to obtain the relaxation time and eq. (5.26) to obtain χ. This quantities can be encountered analytically and substituted in eq. (5.24). Then, it is necessary to minimize the work functional. Before showing an example, we are going to find the relaxation function for the breathing parabola.

5.2.1 Relaxation function for the breathing parabola

Using eqs. (4.9) and (5.21), the generalized force can be written as

$$X = \frac{x^2}{2} \tag{5.27}$$

Then, it follows from eq. (5.22) the relaxation function in this case is given by

$$\Psi(t) = \frac{\beta}{4}(\langle x(0)^2 x(t)^2 \rangle_{eq;\lambda} - \langle x(0)^2 \rangle^2_{eq;\lambda}). \tag{5.28}$$

Therefore, the relaxation function can be found by calculating the correlation between the mean squared position in the equilibrium. In other words, given the initial work parameter, to obtain the relaxation function we must measure/calculate the position, $x(t)$, and obtain the correlation $\langle x(0)^2 x(t)^2 \rangle_{eq;\lambda}$ and the average $\langle x(0)^2 \rangle_{eq;\lambda}$. To obtain an analytical expression, note that the trajectory of a particle in a harmonic potential is given by eq. (3.11). The average in the equilibrium can be found by using the (3.3), (3.2) properties of the thermal noise. Besides, for the initial conditions, x_0 and v_0, it is necessary

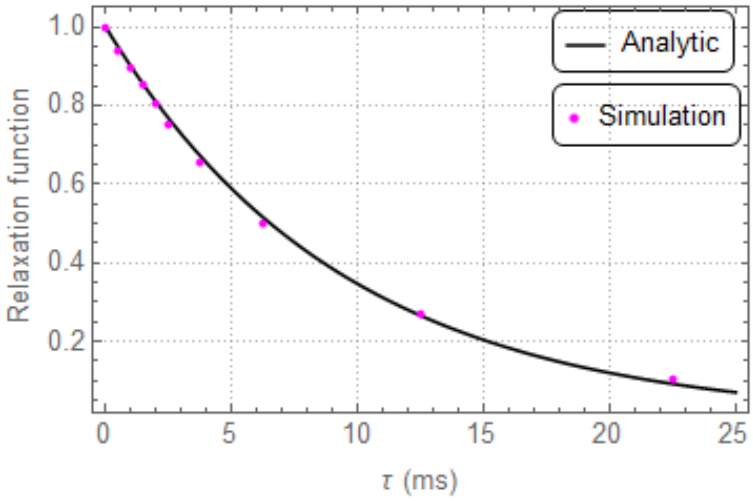

Figure 20 – Comparison between analytic and simulated $\tilde{\Psi}(t) = \Psi(t)/\Psi(0)$ for the breathing parabola. In black/solid the curve is given by eq. (5.29). Dots in magenta are found by simulating the Langevin dynamics and calculating the correlations given by eq. (5.28).

Source: By the author.

to use the information that the system is initially in thermal equilibrium. Therefore, the relaxation function for the breathing parabola in the overdamped regime is equal to

$$\Psi(t) = \Psi(0)\left(\frac{s_2 e^{s_1|t|} - s_1 e^{s_2|t|}}{s_2 - s_1}\right)^2, \tag{5.29}$$

where

$$\Psi(0) = \frac{2}{\beta\lambda^2}, \tag{5.30}$$

$$s_1 = \frac{-\gamma/m - \sqrt{(\gamma/m)^2 - 4(\lambda/m)}}{2}, \tag{5.31}$$

and

$$s_2 = \frac{-\gamma/m + \sqrt{(\gamma/m)^2 - 4(\lambda/m)}}{2}. \tag{5.32}$$

In Figure 20, we compare the relaxation function (eq. (5.29)) found analytically with the relaxation function obtained from the phenomenological approach, i.e., simulating the Langevin equation, measuring positions and then calculating the correlations.

5.2.2 Example: time-dependent stiffness

For the breathing parabola, χ given by eq. (5.26) can be written as

$$\chi(\lambda) = \frac{1}{4}(\langle x(0)^4\rangle_{eq;\lambda} - \langle x(0)^2\rangle^2_{eq;\lambda}) = \frac{1}{2(\beta\lambda)^2}. \tag{5.33}$$

The relaxation time, τ_R, can be re-writen using eqs. (5.25) and (5.29) as

$$\tau_R(\lambda) = \frac{\gamma}{2\lambda}, \tag{5.34}$$

where $m \to 0$, i.e., we considered the overdamped limit. Substituting the above results in the expression of the irreversible work (eq. 5.24), we obtain

$$\langle W_{irr} \rangle = \frac{\gamma(\Delta\lambda)^2}{4\beta\tau\lambda_i^3} \int_0^1 ds \left(\frac{dg}{ds}\right)^2 \frac{1}{\left(1 + \frac{\Delta\lambda}{\lambda_i} g(s)\right)^3} \tag{5.35}$$

The minimum of the functional (again solved using the Euler-Lagrange equation) is found for the protocol

$$g(s) = \frac{-\lambda_i}{\Delta\lambda} + \frac{1}{A(s+B)^2}, \tag{5.36}$$

where A and B are given by the boundary conditions $g(0) = 0$ and $g(1) = 1$. The analysis of such result is in Figure 21. The numerical determination of the performance of this method is part of our first main result. The range of validity of the slowly varying process is not rigorously known. Therefore, the numerical result in Figure 21-d helps to clarify the regime of validity of such a method.

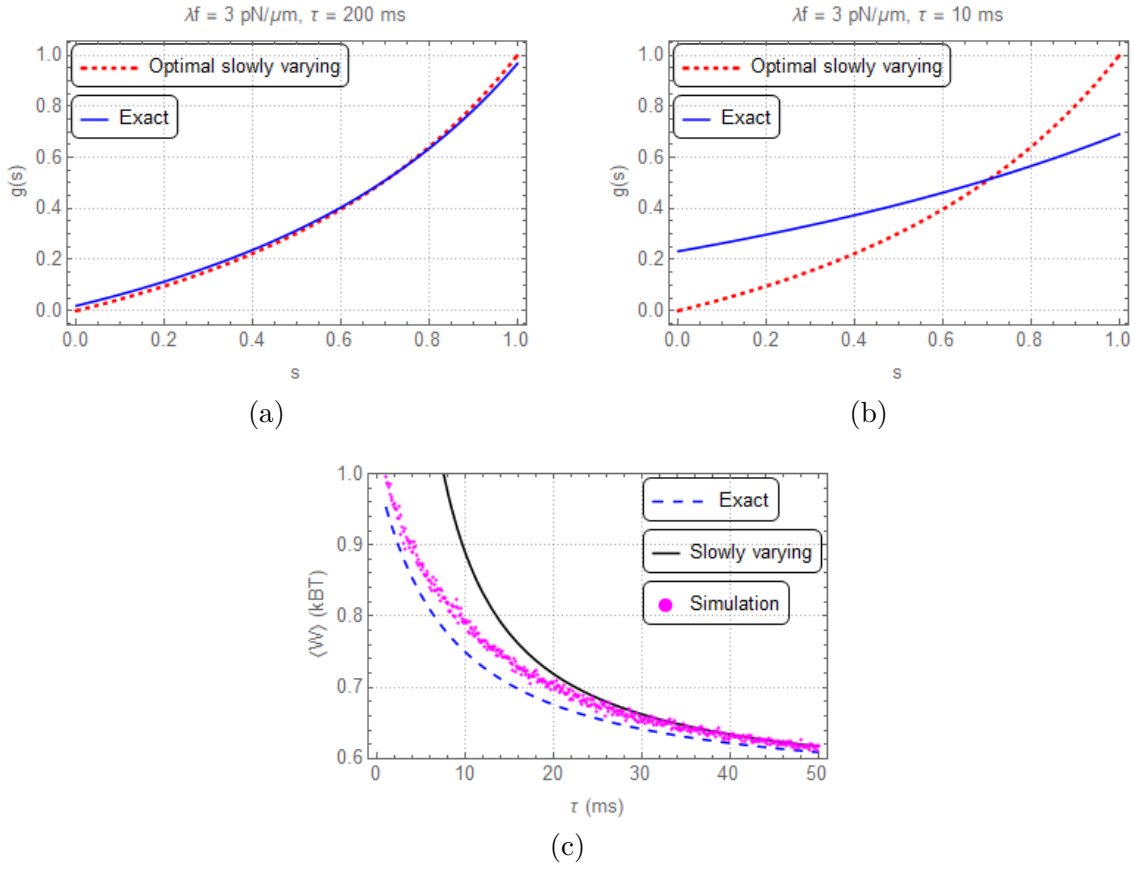

Figure 21 – (a) Comparison between the optimal exact protocol (5.9)(blue/solid) and the protocol for slowly varying processes (5.36)(red/dashed). The protocols agree if the process varies slowly. (b) If the protocol is not a slowly varying process, the protocols have cleary differ. (c) The work decreases with $1/\tau$. In blue/dashed the exact expression for the optimal work (eq. (5.7)), in black/solid the work for slowly varying processes (eq. (5.35)), and dots/magenta the result of the simulation of the Langevin dynamics of the protocol for slowly varying processes (eq. (5.36)). All three curves overlaps at long times, as expected.

Source: By the author.

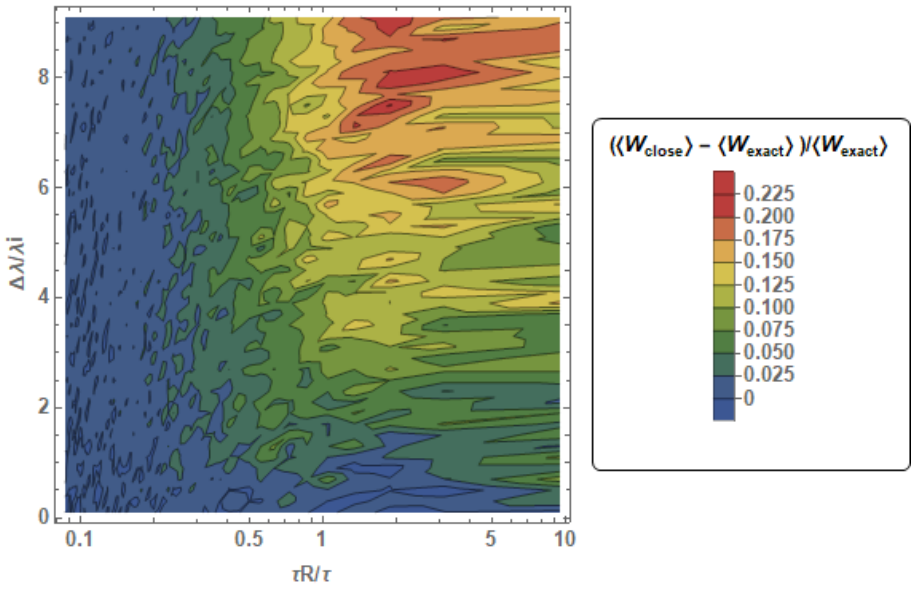

Figure 22 – Relative difference between the optimal protocol for slowly varying processes (eq. (5.24)) and the exact (eq. (5.7)). In other words, the performance (eq. (5.15)) of the protocols for slowly varying processes, for different intensities and switching times. $\tau_R = 9.42$ ms is the relaxation time for when the trap stiffness is equal to λ_i.

Source: By the author.

5.3 Optimal protocols from linear response theory

In the previous section, linear response theory was useful in encountering the optimal protocol for slow processes. Nonetheless, the mean irreversible work also has an expression for weak processes, given by (a deduction is provided in ref. (49))

$$\langle W_{irr}\rangle = \frac{(\Delta\lambda)^2}{2}\int_0^1 ds \int_0^1 ds' \Psi[\tau(s-s')]\frac{dg(s)}{ds}\frac{dg(s')}{ds'}. \tag{5.37}$$

The expression is valid only for the linear response regime. The idea is to expand $dg(s)/ds$ in some basis. Due to its good mathematical properties, a good basis choice is of Chebyshev polynomials, i.e.,

$$\frac{dg(s)}{ds} = \sum_{n=1}^{N} a_n g_{N,n} T_n(2s-1), \tag{5.38}$$

where a_n are the coefficients of the expansion, that will be determined to minimize the work, $T_n(2s-1)$ are the Chebyshev polynomials, and $g_{N,n}$ are factors that regularizes the series expansion (50), due to the Gibbs phenomenon at the extremities of the expansion interval. The factor chosen corresponds to the Jackson kernel and is given by

$$g_{N,n} = \frac{1}{N+1}\left[(N-n+1)\cos\left(\frac{\pi n}{N+1}\right) + \sin\left(\frac{\pi n}{N+1}\right)\cot\left(\frac{\pi}{N+1}\right).\right] \tag{5.39}$$

Substituting the expansion (5.38), into eq. (5.37), we obtain

$$\langle W_{irr}\rangle[(\Delta\lambda)^2\Psi(0)/2]^{-1} = \sum_{n,l}^{N} A_{nl}a_n a_l. \tag{5.40}$$

The coefficients a_n are found by minimizing the above expression, with the constraints $g(0)=0$ and $g(1)=1$. This is done using the Lagrange multipliers method. The physical input in the minimization process is contained in the coefficients A_{nl}:

$$A_{nl} = \int_0^1\int_0^1 \widetilde{\Psi}[\tau(s-s')] \times g_{N,n}g_{N,l}T_n(2s-1)T_l(2s'-1)ds'ds. \tag{5.41}$$

Given the relaxation function, these coefficients can be determined. The main advantage is that the relaxation function can be obtained through experiments, i.e., the details of the microscopic dynamics do not need to be now a priori. Because it is a linear response theory method, theoretically, it is valid only for weak processes (Figure 23). The second main result of this dissertation is the determination of the performance of this method for the breathing parabola, as shown in Figure 25, for different intensities and switching times of the procedure. In addition, we verified the good performance of this method even outside its theoretical regime of validity.

5.3.1 Negative entropy production rate

As we see in section 4.2, the entropy has multiple possible definitions. However, they are not equivalent and presents distinct features. Prigogine showed that the entropy

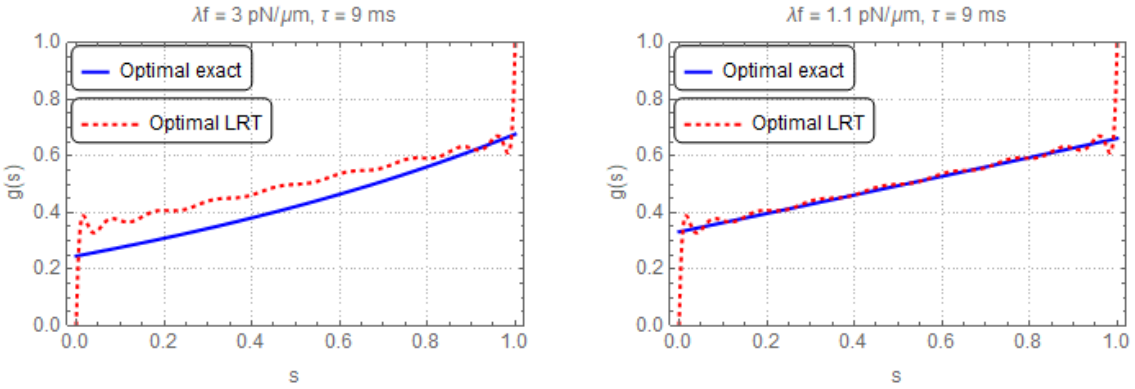

(a) (b)

Figure 23 – Comparison between the protocol (5.9) and the result found by integrating eq. (5.38). The number of terms in the expansion (5.38) is $N = 10$, and the relaxation function is of the breathing parabola (5.29). (a) $\lambda_f = 3$ pN/μm. Because the process is not weak, the protocols have clear differences. (b) $\lambda_f = 1.1$ pN/μm. The protocol is weak, so the protocols are in good agreement.

Source: By the author

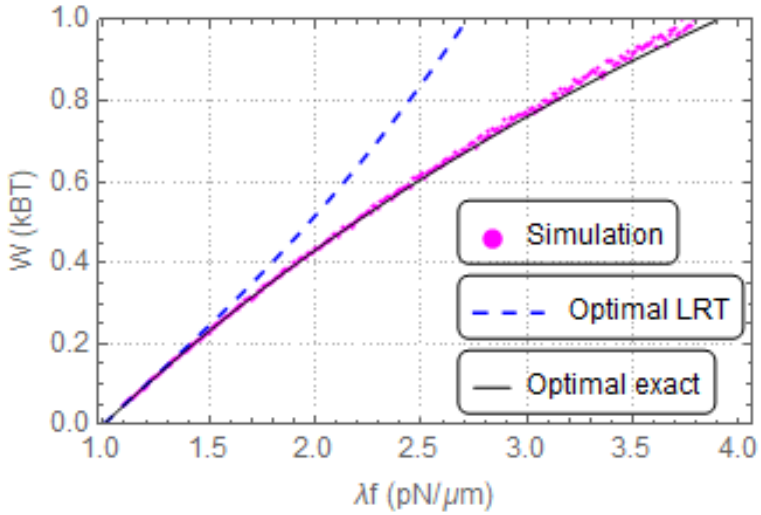

(a)

Figure 24 – Dependence of the average work with λ_f for $\tau = 9$ ms. In blue/dashed, black/solid, and magenta/dots are eqs. (5.40), (5.7), and the average work obtained by simulating the Langevin dynamics with the protocol obtained through the phenomenological method, respectively. It is noteworthy that the protocols generate by the phenomenological method have an average work very close to the optimum. Also, all three curves overlap for λ_f small, as expected.

Source: By the author

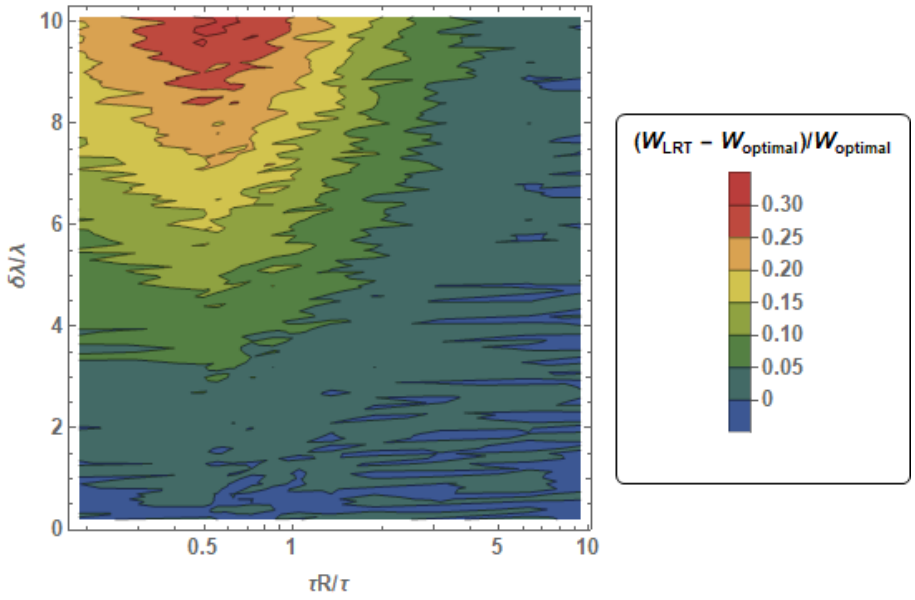

Figure 25 – Performance of the protocols generate by the phenomenological method. Although the protocols were obtained using a linear response theory method, they have good performance even outiside its theoretical regime of validity. The number of terms in expansion (5.38) is equal to 10.

production rate must be positive for retrieving the Second Law of Thermodynamics.(51) From the stochastic entropy defined in section 4.2.1, this is true.(8) Nonetheless, for the measurement of entropy production through the irreversible work, there are negative entropy production rates. The existence of such negative values does not violate the Second Law, as Nazé has shown.(40) Here, we have observed that phenomenological method generates protocols that have negative entropy production rates (Figures 26).

5.3.2 Convergence of the series expansion

In Figure 23, we show a comparison between the approximate phenomenological protocol and the exact optimal protocol. Although the protocols are visually in good agreement, the crucial quantity is the irreversible work value. Moreover, it is interesting to investigate how this value varies with the number of terms in the expansion (5.38). The results are in Figures 27 and 28. We can see that the value of $\sum_{n,l} A_{nl} a_n a_l$ decays when the number of terms increases. Note that the sum seems to converge.

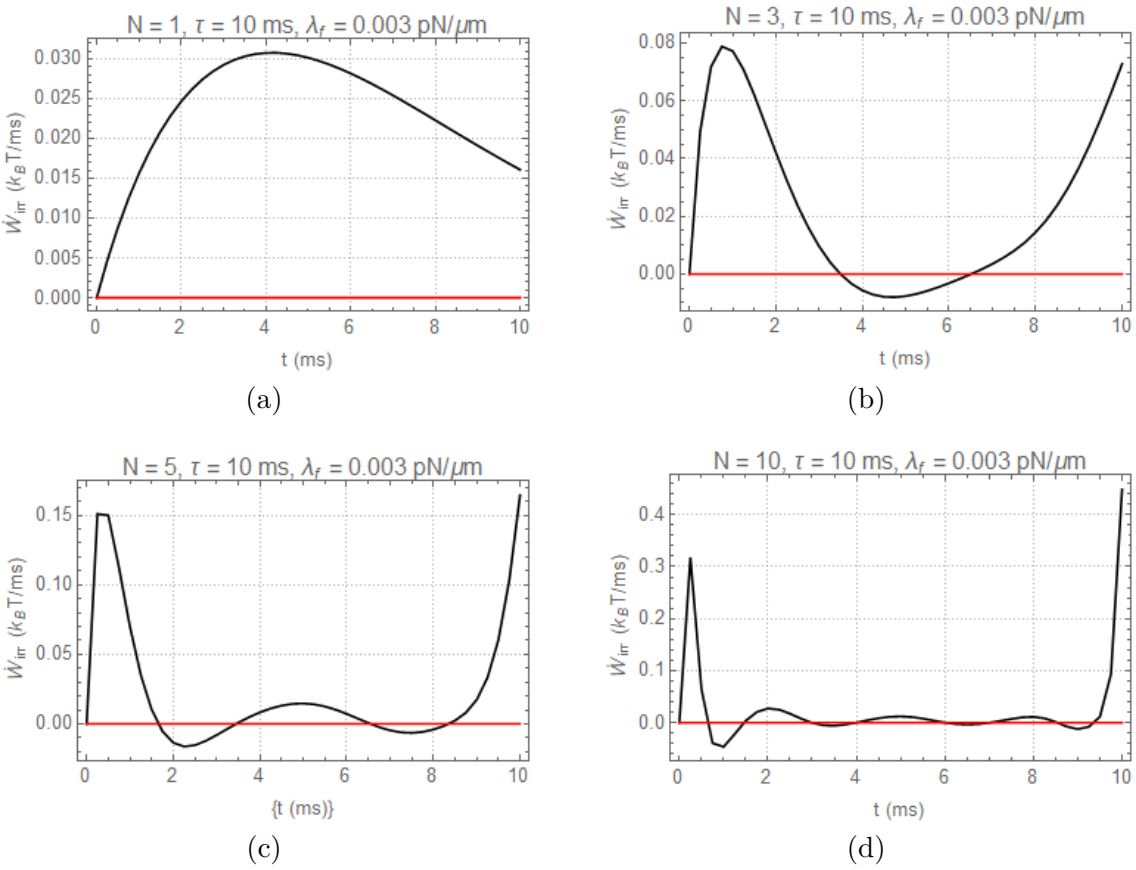

Figure 26 – Comparison of the entropy production rate, $\langle \dot{W}_{irr} \rangle$, for protocols generated using the phenomenological method method. Note that the protocols present negative entropy production rates, and as we increase the number of terms in the expansion, the negative values tend to vanish.

Source: By the author.

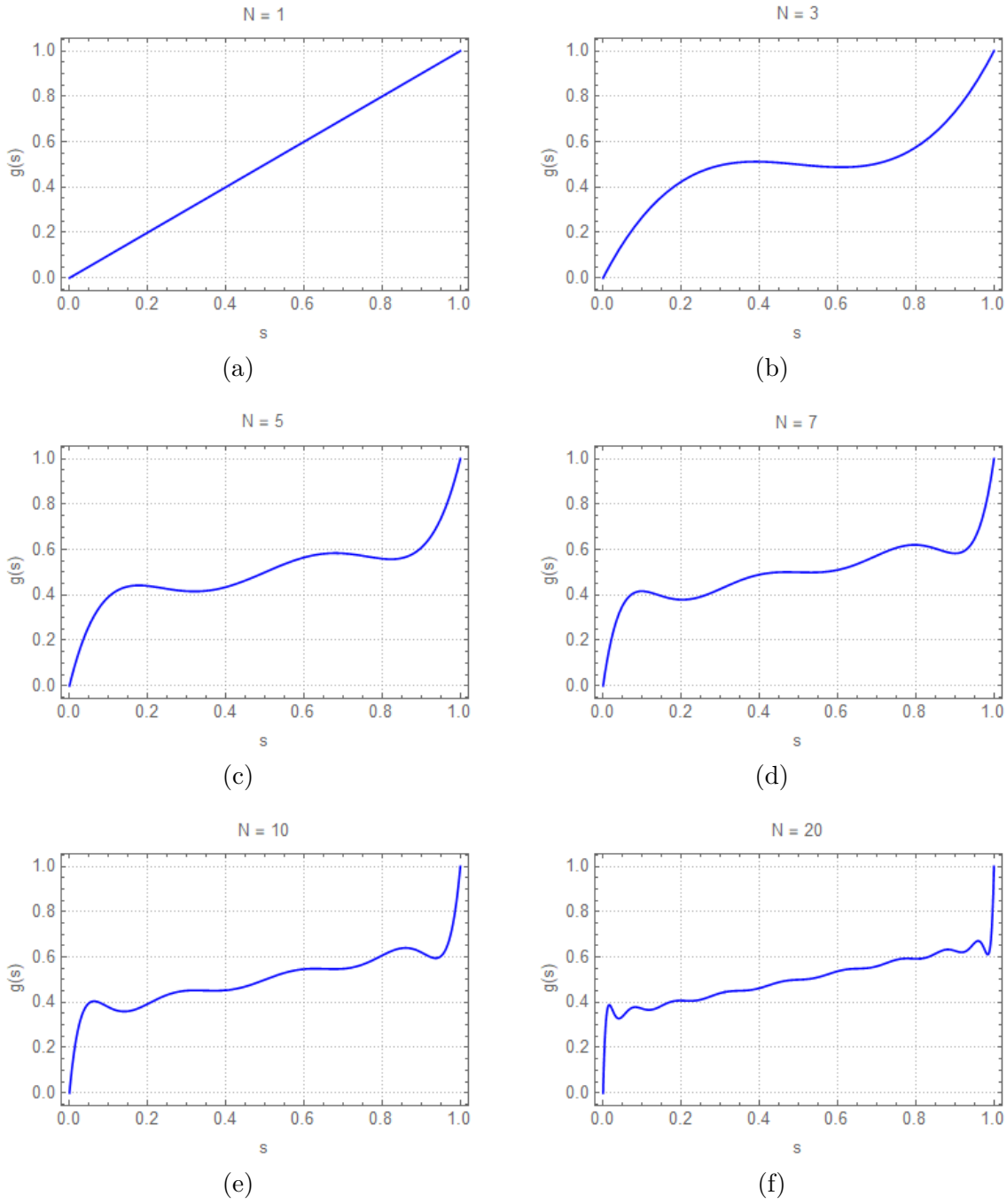

(a) (b) (c) (d) (e) (f)

Figure 27 – Comparison of the protocols generated by the phenomenological method as a function of the number of terms, N, in the expansion (5.38).

Source: By the author.

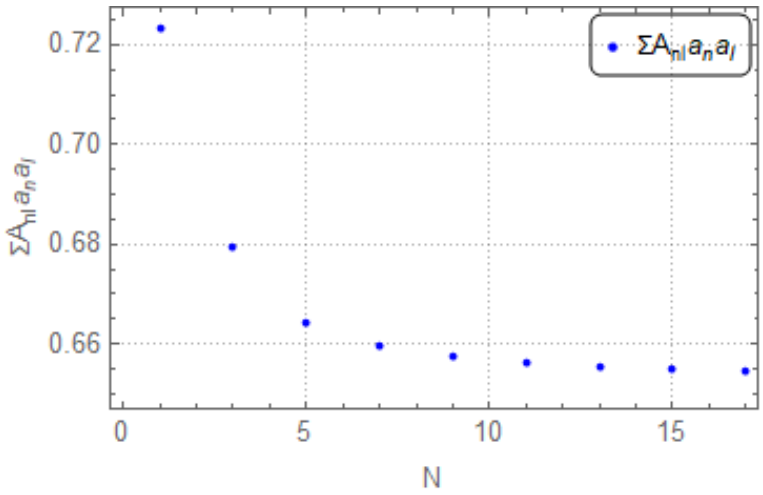

Figure 28 – We see that using more terms in the expansion leads to a diminished value of $\sum_{n,l} A_{nl} a_n a_l$, and consequently, of the irreversible work.

Source: By the author.

5.4 Conclusions

In this chapter, we have studied the optimal processes for a paradigmatic case. Using such a system helps to understand the key features of optimal protocols before attacking more complex problems.

The exact solution provides us a reference value for the optimal work. The difficulties imposed by this analytical procedure lead to the investigation of other methods. For the slowly varying processes, the optimal protocol does not present the characteristic discontinuities of the exact optimal protocol. Also, it does not depend on the switching time.

Then, we studied a phenomenological method for weak processes that allows us to find the optimal protocol if we have the relaxation function of the system. The relaxation function can be measured or deduced, simplifying the optimization problem. We saw that this method may generate protocols that have negative entropy production rates. Also, because this method relies on a finite expansion of the protocol, we studied the dependence of the quantity $\sum_{n,l} A_{nl} a_n a_l$ with the number of terms in the expansion.

6 FEEDBACK CONTROL

In the previous chapter, control of the trap stiffness has allowed us to perform different protocols. The protocols were done independently of the particle's state. If, in addition, the protocol depended on the state of the particle, a problem that dates back from the beginning of classical thermodynamics and that instigated generations of physicists can be studied. The control dependent on the state of the system is called feedback control.

In *Theory of Heat* (19), James C. Maxwell presented a thought experiment, later called Maxwell's demon, to illustrate the statistical character of the Second Law of Thermodynamics. Several discussions about the roles of the information, measurement, and erasure process in this *gedankenexperiment* took place throughout the XX century. The erasure process gained an essential role with Rolf Landauer and Charles Bennett (20, 52), resulting in the Landauer principle: the erasure of 1 bit of information implies at least $k_B T \ln 2$ of heat dissipated. However, the arguments were theoretical. Nowadays, because of the advances in the experiments, such questions can be explored experimentally. First, Berut *et al.* (30), using optical tweezers, verified the Landauer's principle under partial-erasure. Jun, Gavrilov, and Bechhoefer (53) also studied the Landauer's principle. However, they achieved the complete erasure. Toyabe *et al.* (21) verified the information-to-energy conversion, confirmed the generalized Jarzynski equality, and checked both quantities' dependence on the delay time. To accomplish such results, they trapped a colloidal particle in a controlled periodic potential. Paneru *et al.* (54) also verified the information-to-energy conversion. Although, they utilized a brownian particle trapped in a harmonic potential with a time-dependent center-position. Koski *et al.* (55) constructed an autonomous quantum Maxwell demon using coupled single-electron devices. By doing so, they were able to observe an increase in the temperature of the demon. Finally, Saha *et al.* (56) have experimentally accomplished an information engine operating at maximum power and velocity.

In this chapter, we begin by summarizing the discussion of Maxwell's demon. Next, we analyze our simulation of Landauer's principle based on ref. (53) Then, besides verifying some results of the reference (21), we propose a new experiment, which is a simplification of the previous experiments found in the literature. In ref. (21) they experimentally verified the information-to-energy conversion and the generalized Jarzynski equality. The goal of the new experiment is a first step to study such questions in our laboratory. Also, the potential proposed allowed the calculation of the dependence of the information-to-energy conversion with the delay time. In contrast, in ref. (21), they also studied the dependence of the conversion with the delay time but only experimentally.

6.1 Maxwell's demon

Maxwell's demon completed 150 years in 2021. During his lifetime, it was declared exorcized at least three times and caused a lot of discussions about the Second Law of Thermodynamics, entropy, the role of information, and reversible computation. In this quick review, we will follow the classical reference about this subject (57) and divide the timeline into three periods: Maxwell's demon original formulation; the Szilárd's engine and Brillouin argument about the measurement process with light; and the computational approach of Landauer and Bennett, highlighting the role of the erasure process. For a more updated and short review, we refer to (16, 58).

6.1.1 Maxwell's Demon original formulation (1871-1929)

The famous *gedankenexperiment* of Maxwell's demon, which demonstrates the statistical nature of the second law of Thermodynamics, was first presented in Theory of Heat by Maxwell. (19) The idea is to consider a box filled with an ideal gas initially at thermal equilibrium. A wall containing a small door is inserted in the middle of the box. The gatekeeper is a mystical being with the capability of seeing every molecule, allowing the faster ones to go to one side of the vessel and the slower ones into the other, creating a difference of mean velocities of the particles contained in each side of the recipient. Therefore, only by perceiving and handling the particles, the intelligent being is capable of creating a temperature difference, in an apparent violation of the Second Law of Thermodynamics.

6.1.2 Szilard's Engine and Brillouin measurement with light (1929 -1961)

In an article made by Szilárd in 1929 (59), a considerable simplification of the experiment was made. He clarified the importance of the information about the state of the particle, even before the famous article by Claude Shannon introducing the Shannon entropy and information content. (42)

The thought experiment consists of a one-particle ideal gas in a diathermic box in contact with a thermal reservoir. Then, we add a movable partition dividing the recipient into two equal parts. Initially, the wall is kept steady, and the demon measures the side of the particle in the vessel. Next, he allows the expansion of the gas by unfixing the partition. In the expansion process, work is done by the particle. The final state of the particle is equal to its initial state, completing the cycle. Thus, the system in contact with a single heat bath realized work in a cycle, again in an apparent violation of the Second Law of Thermodynamics. Szilard noticed that the value of the work is proportional to $\ln 2$, which is the information (about the side in which the particle is) measured/stored by the demon in a two state system. Thus, he pointed the link between information acquired and the work extracted.

A significant step in this analysis was made in 1951 by Leon Brillouin. (60) He considered that the measurement process used by the demon was via a luminous signal. Besides, he took into account the energetic cost for distinguishing the measurement photon from the thermal radiation of the cavity. The conclusion was that the cost involved in the measurement process compensates for the work obtained in a cycle, temporarily exorcising the demon.

6.1.3 Landauer and Bennett: the computional approach (since 1961)

In 1961, Rolf Landauer argued that for the erasure process in a computer was necessary at least $k_B \ln 2$ of increase of entropy. (20) The previous statement is so important that nowadays is known as Landauer's principle. Years later, Charles Bennett associated the Landauer's principle with Maxwell's demon thought experiment. (52) He argued that the demon was not different from a computer, and erasure of the demon's memory was a crucial step to save the Second Law of Thermodynamics. Besides, relevant arguments were arising about the energetic cost of Brillouin luminous measurement.

6.2 The erasure process and Landauer's principle

As discussed in the previous section, an essential concept in the Maxwell's demon thought experiment is the erasure process, which consists in resetting the system to a predefined state. For example, if there are two states, denoted by "0" and "1", the erasure process of one bit may be defined as the process that takes with certainty any state to the state "0". Landauer's argument leads to that, at least, $k_B T \ln 2$ of work is necessary for erasure one bit of information, i.e.,

$$W_{erasure} \geq k_B T \ln 2.$$

We have simulated the erasure process from ref. (53), where they built an experiment to test the memory model of a particle in a symmetric double-well potential (see Figure 29-a). If the particle is on the left-hand side, the particle is in the state "1". Instead, if it is on the right-hand side, the particle is in the state "0". Therefore, after the complete erasure process, the particle ends up on the right side of the well with a probability equal to 1.

Mathematically, the double-well potential implemented in our model is given by

$$V(x) = 4E_b \left[-\frac{1}{2}(1-\lambda_1)x^2 + \frac{1}{4}x^4 - \alpha\lambda_2 x \right], \tag{6.1}$$

where $E_b = 241.546$ $k_B T$, and $\alpha = 0.5$ μm^{-1}. These values were chosen to make it difficult for the particle to jump through the central barrier and are different from the ones choosen in ref. (53). λ_1 and λ_2 are the control parameters, and the erasure process is made by the following procedure (Figure 29):

1. Step 1. Lowering of the central barrier with a protocol time τ_1 ($\lambda_1 : 0 \to 1$).

2. Step 2. Tilting the potential with a protocol time τ_2 ($\lambda_2 : 0 \to 1$).

3. Step 3. Untilt the potential and rise the barrier simultaneously with a protocol time τ_3 ($\lambda_1 : 1 \to 0$ and $\lambda_2 : 1 \to 0$).

We remark that the processes here are not weak. Also, the three steps above constitute a cycle, with a duration τ_{cycle}. The cycle time is equal to the sum of the duration of each step that is $\tau_{cycle} = \tau_1 + \tau_2 + \tau_3 = 3\tau_1$, where we assumed $\tau_1 = \tau_2 = \tau_3$.

In our simulation, to achieve Landauer's limit, all steps are done slowly to minimize dissipation. Besides, for simplicity, these steps operate with the linear protocol. Since we want to avoid dissipation, we could consider using the optimal protocol instead. But, as already discussed, the exact analytical optimal protocol is generally hard to find. Although the phenomenological linear response theory method validity is for weak processes, one can expect that this method could give a good approximation of the optimal protocol also in this case. However, the optimal protocol in the linear response regime for long switching times is equal to the linear protocol. (61) Therefore, the linear protocol is the best approximation for the optimal protocol with the tools presented in the previous chapter.

The procedure to verify Landauer's principle is to fix a cycle time τ_{cycle} and repeat the erasure process 10000 times, measuring the work required (eqs. (4.8) and (6.1)). Then, change the cycle time and, again, do the erasure process 10000 times. The results are in Figure 30.

We have seen in the previous chapter that for slowly varying processes, irreversible work decays to zero with $1/\tau$ (see eq. (5.24)). So, following the ref. (53), we fit the data in the Figure 30-b with the function,

$$W_{fit}(\tau_{cycle}) = A + \frac{B}{\tau_{cycle}} \tag{6.2}$$

where A and B are constants to be adjusted. The former constant, A, represents the asymptotic value of work and B how fast the convergence is. We have done both the fit for the whole process and each protocol individually and displayed the results in Table 2. Note that choosing the fit function (6.2) based on the argument of slowly varying processes given above is inaccurate. The irreversible work must decay to zero for long times. In other words, the mean work goes to the free energy difference, which due to the erasure process being a cycle, is equal to zero. Hence, the average work tends to zero for very long times. However, in this case, the average work tends to $k_B T \ln 2$. Therefore, we can not justify the fitting function using the theoretical argument for slowly varying processes. Although, we still can use the fit function chosen to find an estimative of Landauer's limit.

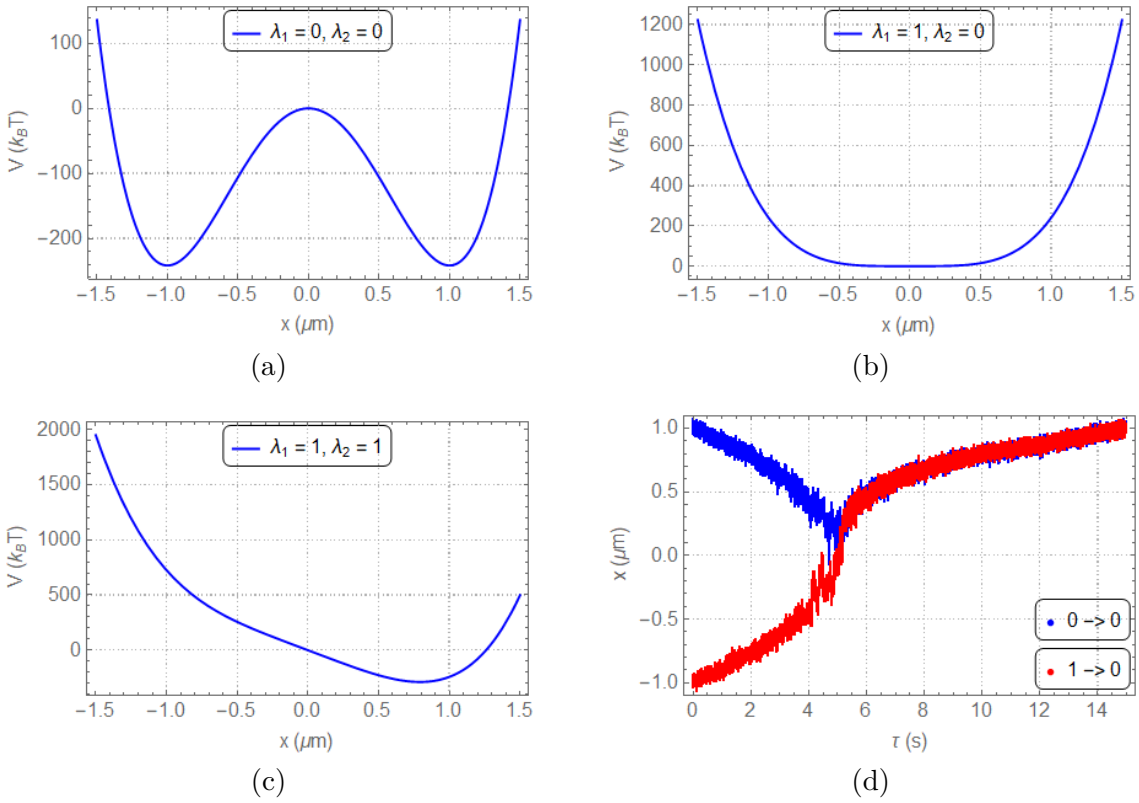

Figure 29 – (a) The particle may be initialized in the left well (state 1) or the right well (state 0). The erasure protocol is defined as the transference of the particle to a predetermined state, in our case, the state 0. (b) In the second step, we lower the middle barrier. (c) Then we tilt the potential to guarantee that the particle ends in the right-hand pit. The final procedure is to undo the changes in the potential. (d) The trajectory of the particle. If initially, it is in state 0, it remains there. Otherwise, it goes to state 0 after the cycle.

Source: By the author.

The irreversible work does not decay to zero because the cycle's time must be slow enough to get closer to the Landauer's limit but sufficiently quick to guarantee that the particle will be in state "0". If the process is very long, the particle will have a chance to end up in state "1", and the work done in the cycle would be smaller than Landauer's limit.

We can see from Table 2 that the essential step is the last one, which must guarantee that the particle ends up in state "0". Note that the work values of the two first steps tend to the free energy difference of the system. Although the last step does not converge to the free energy difference, it tends to the free energy difference plus $k_B T \ln 2$. Thus, the Landauer principle arises from a single step, which is essential for the irreversibility of the cycle.

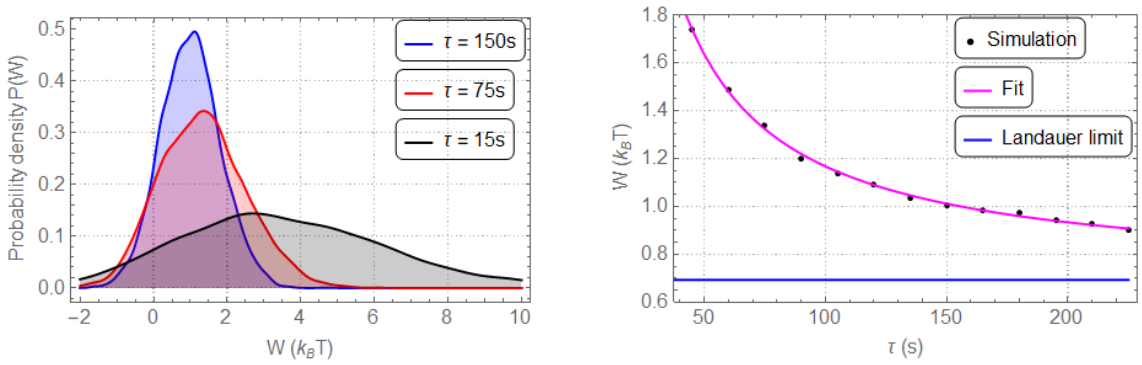

(a) (b)

Figure 30 – (a) Probability density functions for the work for different cycle times. As time increases, the average work diminishes, and the distribution becomes narrower. (b) Average work obtained for different cycle times. Again, as the time increases, the value of work decays to $k_BT \ln 2$, accordingly to the Landauer limit, for complete erasure. Simulation results (dots/black), the fit function (solid/magenta), and the Landauer limit (solid/blue). The constants A and B of the fit are displayed in Table 2.

Source: By the author.

Table 2 – As already said, fitting eq. (6.2) to the simulation data, we obtain A and B. We did this procedure for the cycle as for each step. Note that for steps 1 and 2, the work tends to the free energy, i.e., the asymptotic value of the work, represented by A, is close to the free energy difference. However, in step 3 this does not happen. The work in this step tends to its free energy plus $k_BT \ln 2$ indicating that this step is responsible for the irreversibility. It is easy to imagine that if we did this step more slowly, the particle would have a chance to escape and therefore not erase the information (although the information would be lost). The free energy difference was calculated using equations (4.16) and (6.1). For the entire cycle, the asymptotic value of the work is equal to $A = 1.01 \ln 2$ k_BT, confirming Landauer's limit. Note that the particle is not in a state of thermal equilibrium, and the average work tends to the free energy only because the potential is symmetric.

Step	A (k_BT)	B (k_BT s)	ΔF (k_BT)
1	240.094 ± 0.003	4.7 ± 0.1	240.153
2	-285.452 ± 0.005	10.6 ± 0.2	-285.514
3	46.0574 ± 0.0006	0.24 ± 0.02	45.361
Cycle	0.700 ± 0.006	46.7 ± 0.5	0

Source: By the author

6.3 Information-to-Energy conversion and the generalized Jarzynski equality

In the last section, we have shown the crucial role of the erasure process in Maxwell's demon experiments. Using a double-well potential as our memory model, erasure of one bit required a minimum of $k_B T \ln 2$ of work delivered to the system. Nonetheless, we did not use information about the system's state to extract energy. In this section, we will focus in transforming information into energy by building a Maxwell's Demon. To test the reliability of our simulations, we also verify the generalized Jarzynski equality. Two different potentials were studied: a periodic potential and the "breathing parabola". The former potential was done experimentally by Toyabe *et al.* (21), while the latter is a proposition of a new experiment, to be done in our optical tweezers setup.

6.3.1 Information-to-Energy conversion

Following the ref. (21), consider the potential

$$V(x, \lambda) = A_S x + B_S \cos(\omega x + \lambda), \tag{6.3}$$

where $A_S = 1\ \mathrm{k_B T}\ \cdot\ \mu\mathrm{m}^{-1}$, $B_S = 3\ \mathrm{k_B T}$, and $\omega = 10\ \mu\mathrm{m}^{-1}$ are constants. The coefficient value of A_S used in this dissertation is different from the one used in ref. (21) because the experimental systems are different. The control parameter λ in this case is a phase which varies from 0 to π. The values of the constants were choosen to inhibit the particle changing from potential's wells.

Information about the fluctuations in the medium allows its utilization to extract work and gain free energy. Initially, the particle is in thermal equilibrium in one well of potential $V(x, 0)$ (see Figure 31). At the instant $t_{\mathrm{meas.}}$, the particle position is measured. If the particle is not in region S, nothing happens, and work and the free energy difference are zero. However, if measured in region S (switching region), the potential is changed to $V(x, \pi)$ (Figure 32). The potential switching happens after the measurement, between instants $t_{iswitch}$ and $t_{fswitch}$. The time difference between the measurement and switching is called delay time. The time between the beginning and end of the switching is the protocol time (Figure 33). Here, as a first approximation, we consider that the delay and protocol times are equal to zero. In the reference (21), they studied, experimentally, the relation between information-to-energy conversion and delay time. The conclusion was that control of the conversion was lost for long delay times, as the information about the particle's position becomes outdated.

In the protocol, work is done by the particle while it gains free energy. If the particle was measured in x_1, inside region S, the work is given by (see section 4.1.5)

$$W = V(x_1, \pi) - V(x_1, 0). \tag{6.4}$$

With this equation and Figure 31, it is easy to see that the region S was chosen to make $W < 0$ (remember the convention in section 4.1). Each well has a free energy value

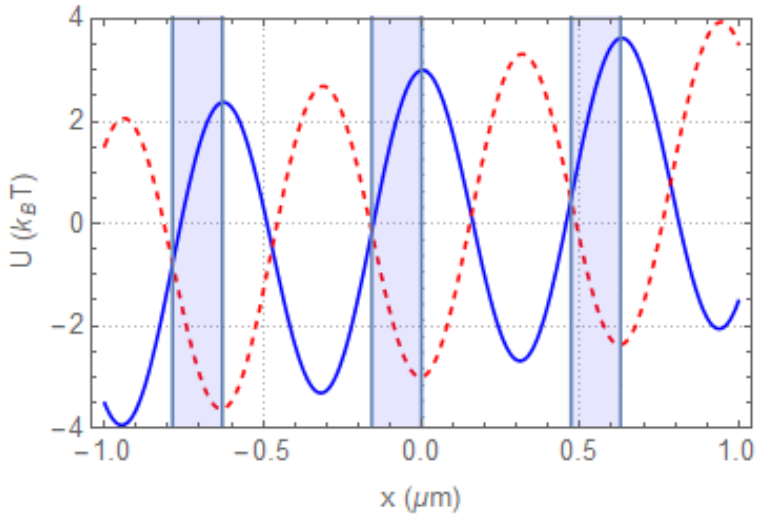

Figure 31 – $V(x,0)$ (solid/blue) and $V(x,\pi)$ (dashed/red). Initially, the particle is in thermal equilibrium in one of the potential wells of $V(x,0)$. If we measure the particle at instant t_{meas} in the highlighted blue area S, the potential energy instantaneously switches to $V(x,\pi)$. In the procedure, the particle does work ($W < 0$) and gains free energy $\Delta F > 0$. The energy obtained comes from the information about the particle's position, representing the information-to-energy conversion.

Source: By the author.

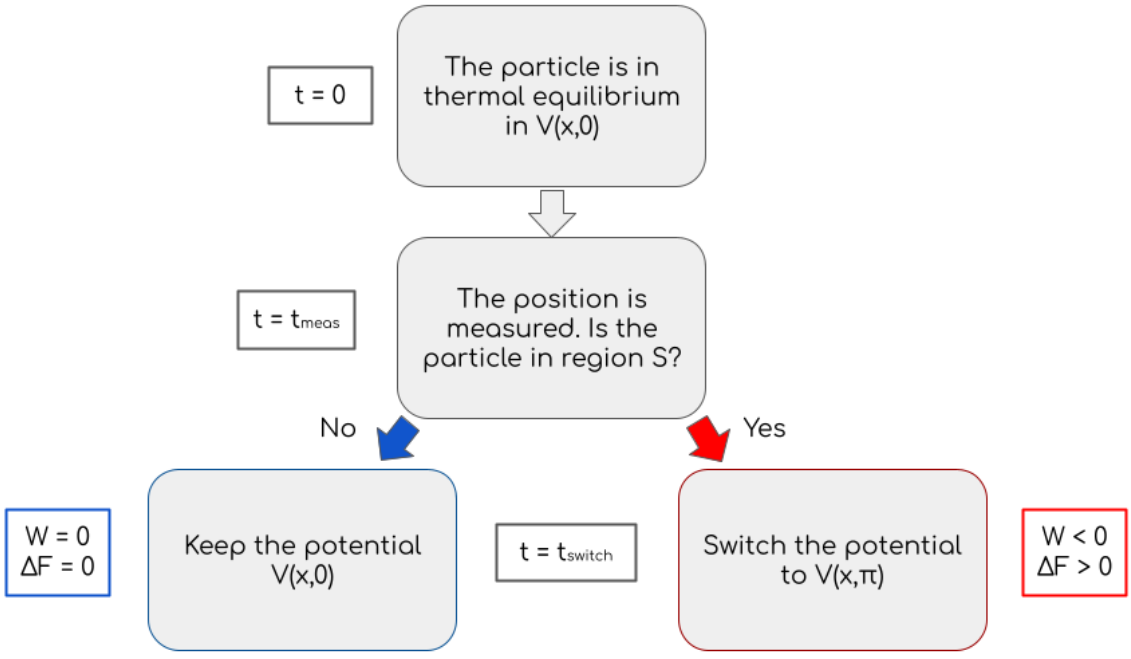

Figure 32 – Procedure to verify the information-to-energy conversion. This kind of control that uses the measurement outcome to decide what protocol to follow, is called feedback control. We repeated this procedure 50000 times to make the average value for the procedure, displayed in Table 3.

Source: By the author.

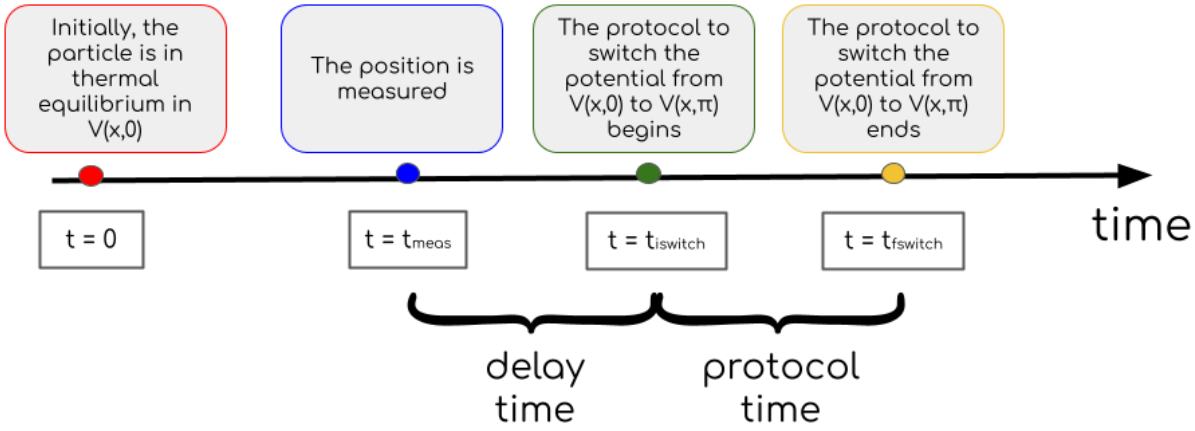

Figure 33 – Timeline of the feedback experiment if the particle is observed in region S.

Source: By the author.

associated and is approximately equal to each pit's energy minimum. It can be obtained using equations (4.16), and (6.3). Because the potential is tilted, the free energy grows for wells in the right direction.

Therefore, realizing this procedure (Figure 34), the particle gains free energy and does work when measured in S. This is called an information-to-energy conversion. We repeat the strategy 50000 times.

Repeating the procedure in Figure 34, the particle climbs the potential. Although impracticable in practice, this is similar to making an object climb stairs without realizing work on it. However, note that the quantities given in Table 3 are average values for procedure.

6.3.2 The efficiency of the information-to-energy conversion

Sagawa, in his thesis (16), showed that when there is information manipulation, the Second Lay of Thermodynamics becomes

$$\langle \Delta F - W \rangle \leq k_B T I, \tag{6.5}$$

where

$$I = -p \ln p - (1-p) \ln (1-p) \tag{6.6}$$

is the Shannon information content, and p is the probability to measure the particle in S. Therefore, there is an energetic cost associated with the manipulation of information, given by k_BTI. The efficiency η of the information-to-energy conversion is defined as,

$$\eta = \frac{\langle \Delta F - W \rangle}{k_BTI}. \tag{6.7}$$

As we always do throughout this dissertation, the results were found by simulating the Langevin dynamics of a colloidal particle. We summarized the results in Table 3. Since there is a delay between measuring and switching in the experiment, in our simulations the efficiency obtained, 0.404, is larger than the encountered in ref. (21).

6.3.3 The generalized Jarzynski equality

The generalized Jarzynski equality or Ueda-Sagawa relation is written as (62)

$$\left\langle \exp\left(\frac{\Delta F - W}{k_BT}\right) \right\rangle = \alpha, \tag{6.8}$$

where α is the efficacy parameter.The efficacy parameter indicates the degree of control that we have over the experiment, and in the case simulated here, its maximum value is two. In the absence of control, its value is equal to 1, recovering the Jarzynski equality. Also, the efficacy parameter is interesting because it can be obtained independently of measurement of work and free energy. It is given by the sum of the probabilities of the particle not being in region S if there is no switching p_{ns}, and of the particle being in region S after the switching p_{sw} (Figure 34). A complete deduction is rather extensive. So, we refer to the Sagawa's thesis for details (16).

Inspecting Table 3, we see that the simulation results agree with the theoretical values. The exception is the generalized Jarzynski equality. Due to the potential shape and definition of region S, there are rare dominant work values. They are responsible for the slow convergence of the generalized Jarzynski equality. Hence, the number of realizations increases compared with the time-dependent stiffness of a harmonic potential. Note that if the particle is close to the potential's maximum, the work will be bigger than if the particle is nearer to a minimum. However, measuring the particle close to the potential's maximum is a rare event because it has to climb the potential driven by the fluctuations.

6.3.4 Theoretical method for instantaneous feedback control

If the particle is, initially, in thermal equilibrium, the Boltzmann weight can be used to calculate all theoretical values in Table 3. If there is a delay time, the problem becomes more complicated because we have to consider the time-evolution of the probability density function between the measure and the switching (given by the Fokker-Planck equation).

Table 3 – Results for the simulation of the feedback experiment realized in ref. (21). The results are in good agreement with each other. The exception is the generalized Jarzynski equality obtained through simulation. The explanation of the dissonant outcome relies on poor statistics, since there are rare dominant rare events (see section 4.4.3). Thus, the number of realizations done was insufficient to verify the generalized Jarzynski equality convergence. For example, the probability to encounter the particle in region S is equal to $p = 0.00976$. This low probability implies that the number of realizations must very large.

Physical quantity	Simulation	Theoretical
$\langle \Delta F - W \rangle$	0.0220 $k_B T$	0.0226 $k_B T$
I	0.0546	0.0549
η	0.403	0.412
$\langle \exp[(\Delta F - W)/k_B T] \rangle$	1.439	1.501
p_{sw}	0.512	0.511
p_{ns}	0.990	0.990
α	1.503	1.501

Source: By the author

For the inverse protocol, the particle is in thermal equilibrium in potential $V(x, \pi)$, then, p_{sw} is found by considering the probability of the particle to be in region S

$$p_{sw} = \frac{\int_S \exp[-V(x,\pi)/k_B T]dx}{\int_{all} \exp[-V(x,\pi)/k_B T]dx}. \tag{6.9}$$

The other quantities are found immediately by considering the particle in thermal equilibrium at potential $V(x, 0)$. The probability for the inverse protocol, where the potential not switch and the particle is not in region S p_{ns} is just equal the probability of the particle not to be in region S:

$$p_{ns} = \frac{\int_{\text{not S}} \exp[-V(x,0)/k_B T]dx}{\int_{all} \exp[-V(x,0)/k_B T]dx}. \tag{6.10}$$

The averages values are equal to

$$\langle \Delta F - W \rangle = \frac{\int_S (\Delta F - W) \exp[-V(x,0)/k_B T]dx}{\int_{all} \exp[-V(x,0)/k_B T]dx}, \tag{6.11}$$

and

$$\langle \exp\left[(\Delta F - W)/k_B T\right] \rangle = \frac{\int_S \exp\left[(\Delta F - W)/k_B T\right] \exp[-V(x,0)/k_B T]dx + \int_{notS} \exp[-V(x,0)/k_B T]dx}{\int_{all} \exp[-V(x,0)/k_B T]dx}, \tag{6.12}$$

where we have used that if the particle is not measured in region S, then $W = \Delta F = 0$.

Of course, the delay time equal to zero is an idealized situation. Toyabe *et al.* investigate how $\langle \Delta F - W \rangle$ and $\langle \exp\left(\frac{\Delta F - W}{k_B T}\right) \rangle$ depended on the delay time as shown in Figures 35 and 36.

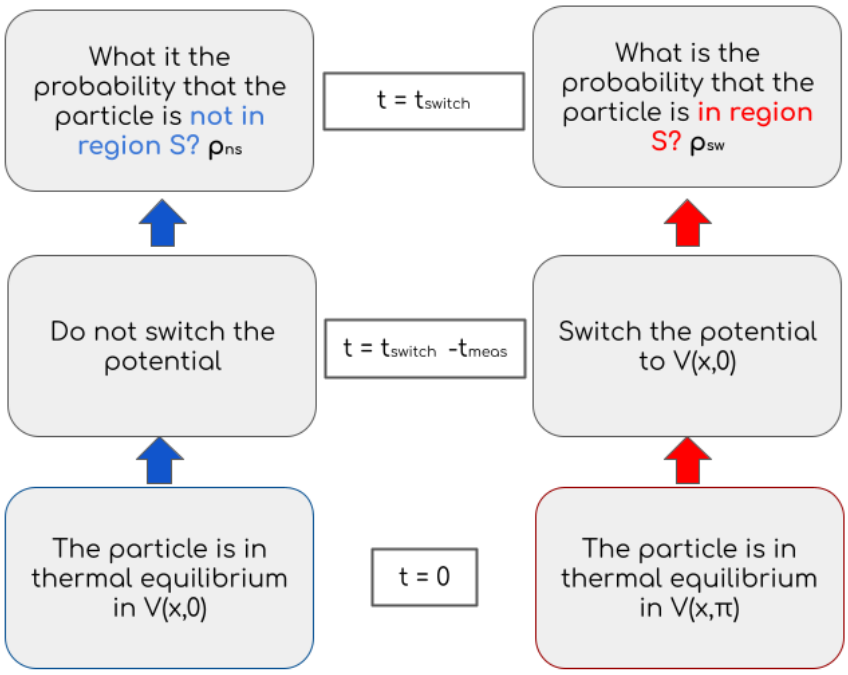

Figure 34 – Reverse feedback experiment. The probabilities p_{ns} and p_{sw} can be obtained independently, allowing the verification of the generalized Jarzynski equality.

Source: By the author.

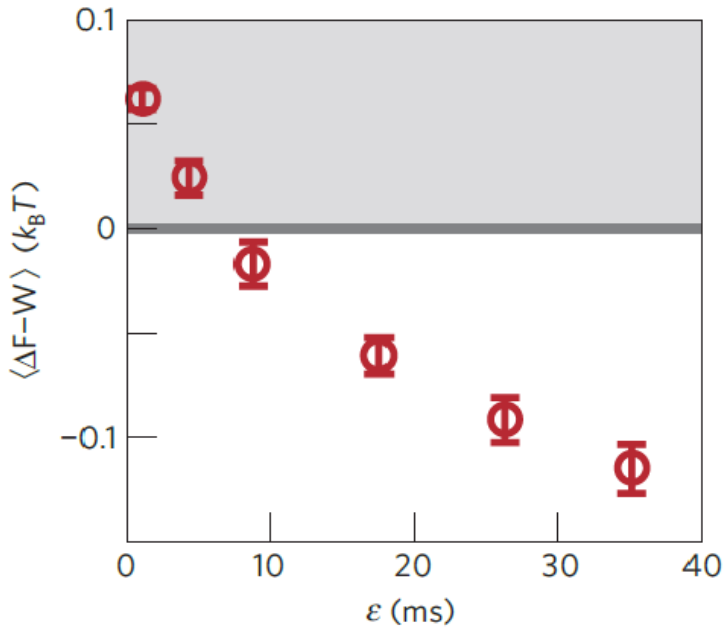

Figure 35 – Dependence of $\langle \Delta F - W \rangle$ with the delay time encountered experimentally by Toyabe *et al.* Observe the notation difference. Here, in this figure, ϵ is the delay time.

Source: Adapted from TOYABE *et al.* (21)

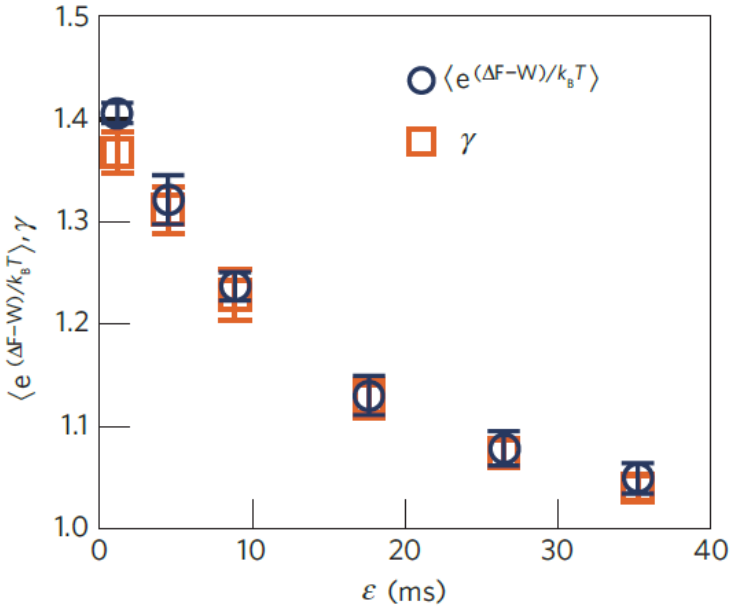

Figure 36 – Dependence of $\langle \exp\left(\frac{\Delta F - W}{k_B T}\right)\rangle$ with the delay time found experimentally by Toyabe *et al.* Observe the notation difference. Here, in this figure, γ is the efficacy parameter.

Source: Adapted from TOYABE *et al.* (21)

6.4 **A new experiment:** the breathing parabola and the information-to-energy conversion

Although the previous potential of ref. (21) can be built in the laboratory, as explained in chapter 2, there is a more immediate potential to study the feedback control. In this context, we thought of a new manner to investigate the information-to-energy conversion with a much simpler setup.

Before showing the proposed experiment, we highlight some features of the previous one. First, given the potential, the switching region is chosen to make $\langle \Delta F - W \rangle > 0$, where $\Delta F > 0$ and $\langle W \rangle < 0$. The size of the region S can not be too narrow since the detector must be able to determine if the particle is in region S or not. Once the particle is measured in region S, the potential is changed. The delay time between measurement and action can not be too large, because the efficiency of the information-to-energy conversion decays with the lag. Last but not least, to obtain the average values of the conversion, the procedure in Figure 32 must be done several times. Although a large number of realizations do not make the experiment impracticable, it makes the experiment cumbersome.

Nowadays, the periodic potential (eq. (6.3)) is not immediately implemented in our laboratory. Thus, a different potential is necessary to explore the information-to-energy conversion. As already said, other factors must be taken into account to verify the feasibility to realize the experiment in practice. Consideration of the number of realizations to the average values converge, the size of the switching region, and the delay between measurement and action all have a relevant role in building a new experiment.

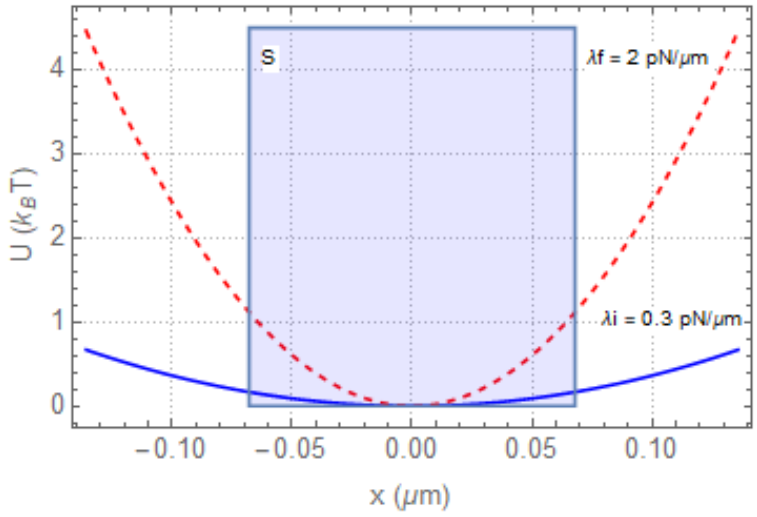

Figure 37 – If the particle is measured in region S at time t_{meas}, the control parameter changes from λ_i to λ_f. Otherwise, nothing happens.

Source: By the author.

Therefore, in this section, we show the potential, the protocol, define a new switching region, study the delay time, and the number of realizations.

Note that in the literature, there are already more complex experiments studying information engines. However, our proposal is a first step to explore in our laboratory this theme.

6.4.1 Experiment description

It is important to remark that the procedure is the same as the previous one (see Figures 32, 33, and 34). The changes are the potential and the switching region. Thus, consider the good and old harmonic potential with time-dependent stiffness

$$V(x,\lambda) = \frac{\lambda x^2}{2}. \tag{6.13}$$

As usual, λ is the control parameter. Initially, the particle is at thermal equilibrium with $\lambda = \lambda_i$. We change the control parameter, from λ_i to λ_f, only if the particle is in the new switching region (see Figure 37). The increase of the trap stiffness means a free energy gain ($\Delta F > 0$), but this time, we must realize work ($W > 0$). Because region S is centralized, the average work for doing such a process is smaller than the average work to do the protocol for all values of x. Therefore, the idea is to use information that the particle is near the center's trap to increase the trap stiffness spending less work. Region S is defined to make the gain in free energy larger than the work spent, i.e., $\Delta F > W$.

6.4.2 Defining the switching region

The stochastic work in the time-dependent stiffness of a harmonic potential grows as further the particle is of the trap's center position. Thus, the switching region is defined to make the free energy difference of the process larger than the maximum value of stochastic work spend $\Delta F > W_{max}$. Mathematically, the borderline value of the position x_S, limiting region S, is given by

$$\Delta F = W_{max}. \tag{6.14}$$

Using eqs. (4.20) and (4.18), we obtain

$$k_B T \ln(\lambda_f/\lambda_i) = \frac{(\lambda_f - \lambda_i)x_S^2}{2}. \tag{6.15}$$

Isolating x_S, the switching region boundary is equal to

$$x_s = \pm\sqrt{\frac{k_B T \ln(\lambda_f/\lambda_i)}{\lambda_f - \lambda_i}}. \tag{6.16}$$

Therefore, the switching region is defined as

$$S = \{x \in \mathbb{R} | -\epsilon x_S < x < \epsilon x_S\}, \tag{6.17}$$

where $\epsilon = 1$ is an adimensional rescale factor. The introduction of this rescale factor will be useful in section 6.4.6 when studying the maximization of $\langle \Delta F - W \rangle$ with the delay time and switching region.

A valid concern is if the QPD has enough resolution to detect the particle in region S. For the parameters chosen in Figure (37), $x_S = 68$ nm. As shown in ref. (27), our spatial resolution is sufficient to determine if the particle is in region S.

In an extreme case, we could choose the region to be infinitely small, centered at the trap's center. In this case, work is zero while the particle gains free energy. However, this is not viable, justifying the definition of a broader switching region.

6.4.3 Number of realizations

The number of realizations of the previous experiment (ref. (21)) was very large compared with the breathing parabola, as studied in section 4.4 to verify the convergence of the generalized Jarzynski equality, as one can see by comparing Figures 16 and 38. As discussed before, in ref. (21) there are rare dominant work values. Therefore, given that the experiment proposed used the breathing parabola, we expect the number of realizations to verify the generalized Jarzynski equality to be much smaller.

6.4.4 Results for the instantaneous protocol

The results for the instantaneous protocol and without delay ($\tau = t_{delay} = 0$) are summarized in Table 4. Remarkably, $\langle \Delta F - W \rangle$ is one order of magnitude larger than

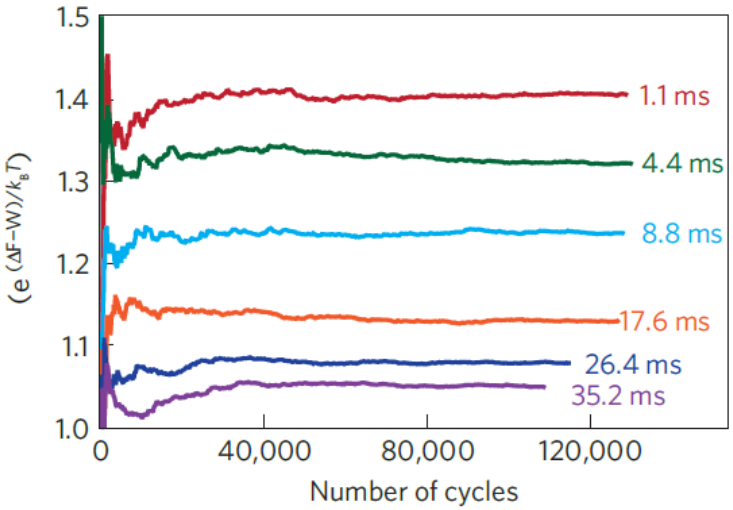

Figure 38 – Convergence of the generalized Jarzynski equality from different delay times found experimentally by Toyabe *et al.* Note the number of realizations (cycles) necessary for convergence is of the order of 10000, value much larger than for the breathing parabola (see section 4.4). The large number is caused by the presence of rare dominant work values. The work values that contribute the most to the convergence are for when the particle is in region S. However, the probability of the particle being in this region is small since it has to climb the potential driven by the fluctuations in the medium. Consequently, the number of realizations to see convergence becomes large.

Source: Adapted from TOYABE *et al.* (21)

Table 4 – Theoretical results of the time-dependent stiffness feedback control of a harmonic potential for $t_{delay} = 0$.

Physical quantity	Theoretical
$\langle \Delta F - W \rangle$	$0.283 k_B T$
I	0.685
η	0.413
$\langle \exp[(\Delta F - W)/k_B T] \rangle$	1.428
p_{sw}	0.865
p_{ns}	0.563
α	1.428

Source: By the author

of ref. (21) because of the large chance of encountering the particle in region S at the switching moment. On the other hand, in ref. (21), in the majority of realizations, the particle was measured outside region S, resulting in a smaller average value. Although $\langle \Delta F - W \rangle$ is larger, I is also one order of magnitude larger, resulting in similar efficiency for the two cases. Note that the values encountered serve as a superior limit for the information-to-energy conversion and efficiency since there is no delay.

6.4.5 Delay time

In practice, neither the delay time nor the protocol time are zero. With our current experimental capabilities, the protocol time can be considered zero, while the delay time can not be neglected. Therefore, we discuss here in more detail the role of the delay in our results.

As a consequence of the potential shape and the definition of region S, we expect the process to be less sensitive to the delay time when compared with the ref. (21). Due to the potential shape, the particle is attracted to the trap's center position (see Figure 37), making it harder to exit region S after the measurement. In the ref. (21), the contrary happens. Since region S includes a maximum of the potential (see Figure 31), the particle receives a force in the direction to expel it from the switching region.

Our main result in this chapter, beyond the proposition of this new simple feedback experiment, is to calculate, theoretically, the dependence of $\langle \Delta F - W \rangle$ with the delay time. This result is essential because it allows a quantitative study about the viability of the experiment. Its noteworthy that Toyabe *et al.* only found the dependence experimentally, as shown in Figures 35 and 36.

Consider that, initially, the particle is at thermal equilibrium in a harmonic potential. Suppose the particle is measured in position x_0 inside region S at $t = 0$. Then, its probability density function becomes $P(x, x_0, 0) = \delta(x - x_0)$. However, from the Fokker-Planck equation solution (eq. (3.32)), we know how this probability density function $P(x, x_0, t)$ evolves during the delay time. Also, after the delay time, the potential is switched instantaneously (see Figure 33). With knowledge about the probability density function above, we can calculate the work (see section 4.1.5). Therefore, the average work if the particle is measured at x_0 is equal to

$$\int_{-\infty}^{\infty} (\Delta F - W) P(x, x_0, t_{delay}) dx. \tag{6.18}$$

However, this is the work contribution only for the particle measured in x_0. To obtain the total average work, we must integrate x_0 in the switching region

$$\langle (\Delta F - W) \rangle = \int_{-x_S}^{x_S} P_{thermal}(x) \left[\int_{-\infty}^{\infty} (\Delta F - W) P(x, x_0, t_{delay}) dx \right] dx_0, \tag{6.19}$$

where $P_{thermal}(x)$ is the thermal equilibrium distribution (eq. (3.33)). The integration is made only in region S, since $W = \Delta F = 0$ if the particle is measured outside S.

Observe that the free energy is given by eq. (4.18) , and the stochastic work is equal to

$$W = \frac{\lambda_f - \lambda_i}{2} x^2 \tag{6.20}$$

in eq. (6.19).

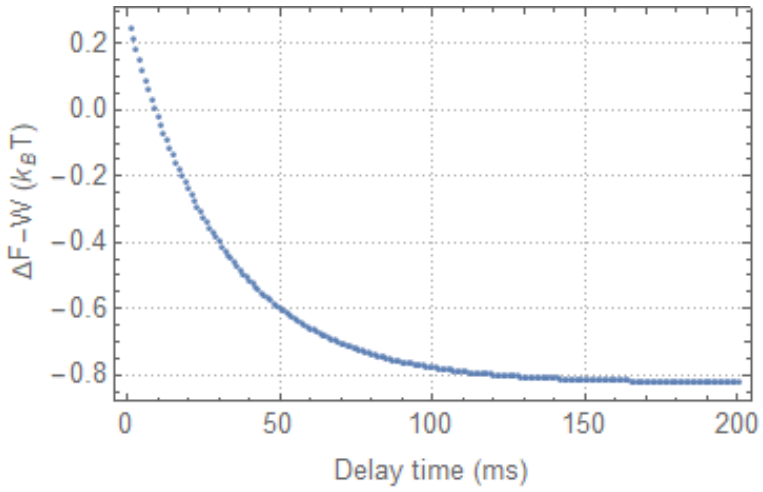

Figure 39 – Dependece of $\langle \Delta F - W \rangle$ with the delay time, calculated using eq. (6.19). $\langle \Delta F - W \rangle$ decays as we increase the delay.

Source: By the author.

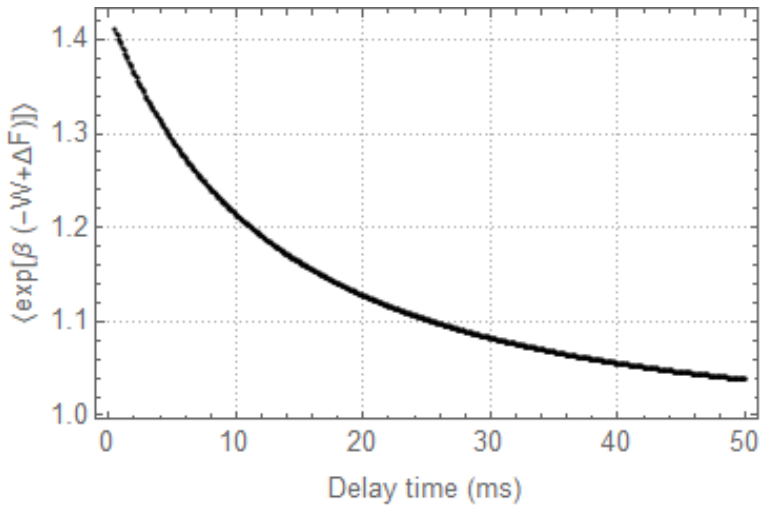

Figure 40 – The generalized Jarzynski equality with the delay time. Note that the value for $\langle \exp[(\Delta F - W)/k_B T] \rangle$ decays, indicating the loss of control of the experiment. It tends to 1 in the long time limit, retrieving the Jarzynski equality. This curve can be calculated similarly to the $\langle \Delta F - W \rangle$ curve.

Source: By the author.

In Figure 39 is the decaying of $\langle \Delta F - W \rangle$ with the delay time. Note that for times below 10 ms the quantity is positive. In Figure 40, the generalized Jarzynski equality. The decay represents a loss in the experiment control.

6.4.6 The switching region

The original definition of the switching region is convenient for an instantaneous process but for a delay time different from zero, measuring the particle in the region S does not guarantee that it will be there in the switching moment. In case that the particle exits

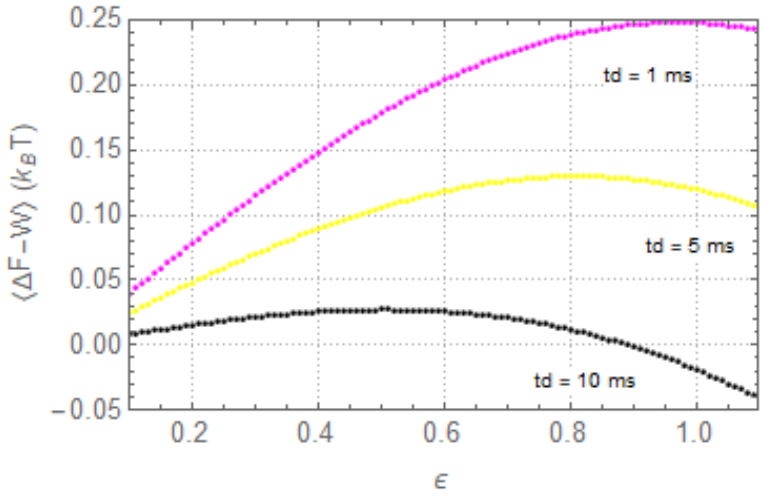

Figure 41 – Relation between $\langle \Delta F - W \rangle$ and ϵ (eq. (6.17)) for different delay times. The larger the delay time, the smaller the value of ϵ that maximizes $\langle \Delta F - W \rangle$.

Source: By the author.

the switching region during the delay time, it will have $W > \Delta F$, decreasing the average $\langle \Delta F - W \rangle$. Therefore, to achieve the maximum of $\langle \Delta F - W \rangle$ is necessary to define a new switching region. The scaling factor, ϵ, is used to study other possibilities of the switching region.

Fixing the delay time and considering that the particle was measured in region S, three aspects come into play in the maximization of $\langle \Delta F - W \rangle$: 1) if $\epsilon > 1$, there will be negative values of $\Delta F - W$, decreasing the average value $\langle \Delta F - W \rangle$; 2) if $\epsilon < 1$, the value obtained for $\Delta F - W$ is positive because the particle does not have time to exit the region S; 3) if the region is too small $\epsilon \ll 1$, positive values $\langle \Delta F - W \rangle$ that contributes to the average are lost, again decreasing the average. Therefore, to maximize $\langle \Delta F - W \rangle$, a smaller switching region must be considered. Also, the region S can not be too small for the reasoning above.The results are in Figures 41 and 42.

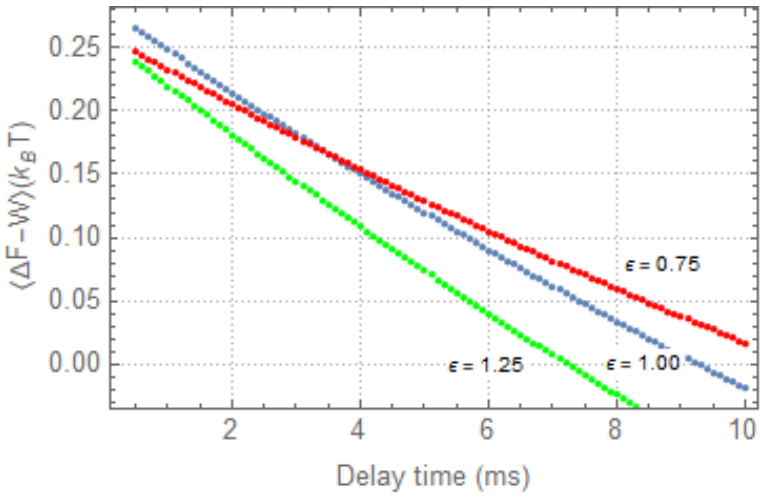

Figure 42 – $\langle \Delta F - W \rangle$ with the delay time, for different scaling factors of the interval S. For $\epsilon = 1.25$ (green), $\langle \Delta F - W \rangle$ is smaller for all delay times. For $\epsilon = 1.00$ (blue), $\langle \Delta F - W \rangle$ is larger for a small delay. When we increase the delay time, this curve rapidly decays because there is a probability that the particle will exit region S. For $\epsilon = 0.75$ (red), $\langle \Delta F - W \rangle$ does not have the larger value for short delay times but decays more slowly.

Source: By the author.

7 CONCLUSION

In the last years, an optical tweezer was developed in our laboratory.(27) Among several possibilities that this experimental setup allows, in this dissertation, we choose to explore some themes of the broad and rich field of stochastic thermodynamics. Although the study made be mainly theoretical and computational, we sought to study and propose possible experiments to be realized in practice soon. Hence, we began showing the basic features of the experimental system, such as the type of object we trap, the force's intensities, and the time scales. Given that we trap a colloidal particle immersed in water, we developed the theory that describes the particle's motion, i.e., the Langevin equation and the Fokker-Planck equation. In addition, we introduce ref. (34), which explains how to simulate the Langevin dynamics. These simulations were of great help in clarifying concepts and verifying the feasibility of experiments.

Nonetheless, the Langevin and Fokker-Planck equations do not introduce the concepts of work, heat, and entropy. Thus, we presented the work of Ken Sekimoto that, in 1998, associated to individual trajectories of a Brownian particle the concepts of work and heat.(10) These thermodynamic quantities fluctuate, i.e., different realizations of the experiment give different values for the work and heat. However, the probability distributions obey important relations, known as fluctuation theorems, being the Jarzynski equality the most famous.(5) In our case, the Jarzynski equality was useful as a simulation checker and, since the JE is an average of the exponential of the work, some values contribute more to the average process, interfering in the number of times that the experiment must be done to see JE convergence. Therefore, we investigate if the so-called dominant work values were also rare events or not for the breathing parabola.

Although in stochastic thermodynamics work becomes a quantity that fluctuates between realizations of the experiment, the average work is always larger than the free energy difference of the system. The optimal protocol has the mean work the closest to ΔF. We have studied three different methods to obtain the optimal protocol for the harmonic potential with time-dependent stiffness. The first method generates an exact analytical solution (15), while one is for slowly varying processes (17), and the last is a phenomenological method for weak protocols.(18) Our contribution was the determination of the performance of the two last methods. In particular, the phenomenological method presented a good performance even outside its theoretical regime of validity.

Last we have explored Landauer's principle and the information-to-energy conversion. For the former, we reproduced the results of ref. (53). As for the latter, we reproduced the results of the ref. (21), where they verified the information-to-energy conversion as the generalized Jaryznski equality. Our second main result is that we have proposed a new

similar experiment but more easily implemented. This simplicity allowed the calculation of the dependence of $\langle \Delta F - W \rangle$ with the delay time, i.e., the time between the measurement the potential change. Although Toyabe *et al.* have already studied how the delay time affects the information-to-energy conversion, they did this experimentally. Hence, we made a little advancement by calculating this time dependence theoretically.

Therefore, we hope that the discussions and results encountered in this dissertation, concerning the optimization of protocols and the feedback control, serve as a useful guide in our laboratory group in the following years.

REFERENCES

1 CARNOT, S. **Réflexions sur la puissance motrice du feu**. Paris: Vrin, 1978.

2 CALLEN, H. B. **Thermodynamics and an introduction to thermostatistics**. 2nd ed. New York: Wiley, 1998.

3 REICHL, L. E. **A modern course in statistical physics**. 2nd ed. New York: Wiley, c1998.

4 KUBO, R.; TODA, M.; HASHITSUME, N. **Statistical physics II:** nonequilibrium statistical mechanics. 2nd ed. Berlin: Springer, 2012. (Solid state sciences, v.31).

5 JARZYNSKI, C. Equilibrium free-energy differences from nonequilibrium measurements: a master-equation approach. **Physical Review E**, APS, v. 56, n. 5, p. 5018, 1997.

6 CROOKS, G. E. Entropy production fluctuation theorem and the nonequilibrium work relation for free energy differences. **Physical Review E**, APS, v. 60, n. 3, p. 2721, 1999.

7 HATANO, T.; SASA, S.-i. Steady-state thermodynamics of langevin systems. **Physical Review Letters**, APS, v. 86, n. 16, p. 3463, 2001.

8 SEIFERT, U. Entropy production along a stochastic trajectory and an integral fluctuation theorem. **Physical Review Letters**, APS, v. 95, n. 4, p. 040602, 2005.

9 SPECK, T.; SEIFERT, U. Integral fluctuation theorem for the housekeeping heat. **Journal of Physics A:** mathematical and general, IOP Publishing, v. 38, n. 34, p. L581, 2005.

10 SEKIMOTO, K. Langevin equation and thermodynamics. **Progress of Theoretical Physics Supplement**, Oxford Academic, v. 130, p. 17–27, 1998. DOI: 10.1143/PTPS.130.17.

11 COLLIN, D. et al. Verification of the crooks fluctuation theorem and recovery of RNA folding free energies. **Nature**, Nature Publishing Group, v. 437, n. 7056, p. 231–234, 2005.

12 MARTÍNEZ, I. *et al.* Brownian carnot engine. **Nature Physics**, Nature publishing group, v. 12, n. 1, p. 67–70, 2016.

13 NOVIKOV, I. The efficiency of atomic power stations (a review). **Journal of Nuclear Energy (1954)**, Elsevier, v. 7, n. 1-2, p. 125–128, 1958.

14 CURZON, F. L.; AHLBORN, B. Efficiency of a carnot engine at maximum power output. **American Journal of Physics**, American Association of Physics Teachers, v. 43, n. 1, p. 22–24, 1975.

15 SCHMIEDL, T.; SEIFERT, U. Optimal finite-time processes in stochastic thermodynamics. **Physical Review Letters**, APS, v. 98, n. 10, p. 108301, 2007.

16 SAGAWA, T. Thermodynamics of information processing in small systems. **Progress of Theoretical Physics**, Oxford University Press, v. 127, n. 1, p. 1–56, 2012.

17 BONANÇA, M. V.; DEFFNER, S. Optimal driving of isothermal processes close to equilibrium. **Journal of Chemical Physics**, American Institute of Physics, v. 140, n. 24, p. 244119, 2014.

18 BONANÇA, M. V.; DEFFNER, S. Minimal dissipation in processes far from equilibrium. **Physical Review E**, APS, v. 98, n. 4, p. 042103, 2018.

19 MAXWELL, J. C.; PESIC, P. **Theory of heat**. Massachusetts: Courier Corporation, 2001.

20 LANDAUER, R. Irreversibility and heat generation in the computing process. **IBM Journal of Research and Development**, Ibm, v. 5, n. 3, p. 183–191, 1961.

21 TOYABE, S. *et al.* Experimental demonstration of information-to-energy conversion and validation of the generalized jarzynski equality. **Nature Physics**, Nature Publishing Group, v. 6, n. 12, p. 988–992, 2010.

22 ASHKIN, A. Acceleration and trapping of particles by radiation pressure. **Physical Review Letters**, APS, v. 24, n. 4, p. 156, 1970.

23 ASHKIN, A. *et al.* Observation of a single-beam gradient force optical trap for dielectric particles. **Optics Letters**, Optical Society of America, v. 11, n. 5, p. 288–290, 1986.

24 ASHKIN, A. Atomic-beam deflection by resonance-radiation pressure. **Physical Review Letters**, APS, v. 25, n. 19, p. 1321, 1970.

25 RITORT, F. Single-molecule experiments in biological physics: methods and applications. **Journal of Physics:** condensed matter, IOP Publishing, v. 18, n. 32, p. R531, 2006.

26 SEIFERT, U. Stochastic thermodynamics, fluctuation theorems and molecular machines. **Reports on Progress in Physics**, IOP Publishing, v. 75, n. 12, p. 126001, 2012.

27 MARTINS, T. T. **Aprisionamento óptico de micropartículas e desenvolvimento de potenciais ópticos dinâmicos**. 2019. 163 p. Dissertação (Mestrado em Ciências) — Instituto de Fısica de São Carlos, Universidade de São Paulo, São Carlos, 2019.

28 JONES, P. H.; MARAGÒ, O. M.; VOLPE, G. **Optical tweezers:** principles and applications. Cambridge: Cambridge University Press, 2015.

29 ALBAY, J. *et al.* Optical tweezers as a mathematically driven spatio-temporal potential generator. **Optics Express**, Optical Society of America, v. 26, n. 23, p. 29906–29915, 2018.

30 BÉRUT, A. *et al.* Experimental verification of landauer's principle linking information and thermodynamics. **Nature**, Nature Publishing Group, v. 483, n. 7388, p. 187–189, 2012.

31 MARTINS, T. T.; MUNIZ, S. R. Dynamically controlled double-well optical potential for colloidal particles. *In*: SBFOTON INTERNATIONAL OPTICS AND PHOTONICS CONFERENCE (SBFOTON IOPC), 2021, São Carlos. **Anais** [. . .].Piscataway: IEEE, 2021. DOI: 10.1109/SBFotonIOPC50774.2021.9461866.

32 BOYCE, W. E.; DIPRIMA, R. C.; MEADE, D. B. **Elementary differential equations**. New York: John Wiley & Sons, 2017.

33 OKSENDAL, B. **Stochastic differential equations: an introduction with applications**. 6th ed. Heidelberg: Springer Science & Business Media, 2013.

34 VOLPE, G.; VOLPE, G. Simulation of a brownian particle in an optical trap. **American Journal of Physics**, American Association of Physics Teachers, v. 81, n. 3, p. 224–230, 2013.

35 RILEY, K. F.; HOBSON, M. P.; BENCE, S. J. **Mathematical methods for physics and engineering**. Cambridge: Cambridge University Press, 1997.

36 VILAR, J. M.; RUBI, J. M. Failure of the work-hamiltonian connection for free-energy calculations. **Physical Review Letters**, APS, v. 100, n. 2, p. 020601, 2008.

37 HOROWITZ, J.; JARZYNSKI, C. Comment on "failure of the work-hamiltonian connection for free-energy calculations". **Physical Review Letters**, APS, v. 101, n. 9, p. 098901, 2008.

38 PELITI, L. Comment on "failure of the work-hamiltonian connection for free-energy calculations". **Physical Review Letters**, APS, v. 101, n. 9, p. 098903, 2008.

39 PELITI, L. On the work–hamiltonian connection in manipulated systems. **Journal of Statistical Mechanics:** theory and experiment, IOP Publishing, v. 2008, n. 05, p. P05002, 2008.

40 NAZÉ, P.; BONANÇA, M. V. Compatibility of linear-response theory with the second law of thermodynamics and the emergence of negative entropy production rates. **Journal of Statistical Mechanics:** theory and experiment, IOP Publishing, v. 2020, n. 1, p. 013206, 2020.

41 BONANÇA, M. V.; DEFFNER, S. Fluctuation theorem for irreversible entropy production in electrical conduction. **arXiv preprint arXiv:2110.03381**, 2021.

42 SHANNON, C. E. A mathematical theory of communication. **The Bell System Technical Journal**, Nokia Bell Labs, v. 27, n. 3, p. 379–423, 1948.

43 JARZYNSKI, C. Nonequilibrium equality for free energy differences. **Physical Review Letters**, APS, v. 78, n. 14, p. 2690, 1997.

44 JARZYNSKI, C. Rare events and the convergence of exponentially averaged work values. **Physical Review E**, APS, v. 73, n. 4, p. 046105, 2006.

45 HALPERN, N. Y.; JARZYNSKI, C. Number of trials required to estimate a free-energy difference, using fluctuation relations. **Physical Review E**, APS, v. 93, n. 5, p. 052144, 2016.

46 SPECK, T. Work distribution for the driven harmonic oscillator with time-dependent strength: exact solution and slow driving. **Journal of Physics A:** mathematical and theoretical, IOP Publishing, v. 44, n. 30, p. 305001, 2011.

47 GOMEZ-MARIN, A.; SCHMIEDL, T.; SEIFERT, U. Optimal protocols for minimal work processes in underdamped stochastic thermodynamics. **Journal of Chemical Physics**, American Institute of Physics, v. 129, n. 2, p. 024114, 2008.

48 SIVAK, D. A.; CROOKS, G. E. Thermodynamic metrics and optimal paths. **Physical Review Letters**, APS, v. 108, n. 19, p. 190602, 2012.

49 ACCONCIA, T. V.; BONANÇA, M. V. Degenerate optimal paths in thermally isolated systems. **Physical Review E**, APS, v. 91, n. 4, p. 042141, 2015.

50 WEISSE, A. *et al.* The kernel polynomial method. **Reviews of Modern Physics**, APS, v. 78, n. 1, p. 275, 2006.

51 PRIGOGINE, I. **Introduction to thermodynamics of irreversible processes**. New York: Interscience, 1967.

52 BENNETT, C. H. The thermodynamics of computation—a review. **International Journal of Theoretical Physics**, Springer, v. 21, n. 12, p. 905–940, 1982.

53 JUN, Y.; GAVRILOV, M.; BECHHOEFER, J. High-precision test of landauer's principle in a feedback trap. **Physical Review Letters**, APS, v. 113, n. 19, p. 190601, 2014.

54 PANERU, G. *et al.* Lossless brownian information engine. **Physical Review Letters**, APS, v. 120, n. 2, p. 020601, 2018.

55 KOSKI, J. V. *et al.* On-chip maxwell's demon as an information-powered refrigerator. **Physical Review Letters**, APS, v. 115, n. 26, p. 260602, 2015.

56 SAHA, T. K. *et al.* Maximizing power and velocity of an information engine. **Proceedings of the National Academy of Sciences**, National Acad Sciences, v. 118, n. 20, p. e2023356118, 2021.

57 LEFF, H.; REX, A. F. **Maxwell's demon 2 entropy, classical and quantum information, computing**. Boca Raton: CRC Press, 2002.

58 LUTZ, E.; CILIBERTO, S. From maxwells demon to landauers eraser. **Physics Today**, v. 68, n. 9, p. 30, 2015.

59 SZILARD, L. On the decrease of entropy in a thermodynamic system by the intervention of intelligent beings. **Behavioral Science**, Wiley Online Library, v. 9, n. 4, p. 301–310, 1964.

60 BRILLOUIN, L. Maxwell's demon cannot operate: information and entropy. I. **Journal of Applied Physics**, American Institute of Physics, v. 22, n. 3, p. 334–337, 1951.

61 NAZÉ, P. M. A. L. **Thermodynamic aspects in linear response theory**. 2021. Thesis (Doctor in Science) — Instituto de Fısica Gleb Wataghin, Universidade Estadual de Campinas, Campinas, 2021.

62 SAGAWA, T.; UEDA, M. Generalized jarzynski equality under nonequilibrium feedback control. **Physical Review Letters**, APS, v. 104, n. 9, p. 090602, 2010.